Transportation Research Part E 157 (2022) 102492

Contents lists available at ScienceDirect

Transportation Research Part E

journal homepage: www.elsevier.com/locate/tre

Energy-efficient high-speed train rescheduling during a major disruption

Shuguang Zhan [a,*], Pengling Wang [b,*], S.C. Wong [c,d], S.M. Lo [e]

[a] School of Transportation and Logistics, Southwest Jiaotong University, Chengdu 610031, Sichuan, China
[b] College of Transportation Engineering, Tongji University, Shanghai, China
[c] Department of Civil Engineering, The University of Hong Kong, Pokfulam Road, Hong Kong
[d] Guangdong - Hong Kong - Macau Joint Laboratory for Smart Cities
[e] Department of Architecture and Civil Engineering, City University of Hong Kong, Kowloon, Hong Kong

ARTICLE INFO

Keywords:
High-speed railway
Energy saving
Train rescheduling
Integer linear programming

ABSTRACT

Disruptions are inevitable in daily train operations, and can cause high-speed trains to deviate from their official schedules. Therefore, the efficient rescheduling of disrupted trains is critical for ensuring smooth daily operations. We sought to determine the appropriate arrival and departure times and orders of trains at each station during a disruption, and the speed profile of each train, to reduce the delay costs and energy consumption. To embed the train speed profile corresponding to energy saving into the train rescheduling problem, a space–time–speed network is applied for problem formulation. Thus, the energy-efficient train speed profile is embedded in the speed dimension in the space–time–speed hypernetwork. The detailed train speed profile between two stations is formulated as a multiple-phase optimal control model, which is solved using a pseudospectral method. Then, an integer linear programming model based on multicommodity flow is built to solve the train rescheduling problem. We decompose it via the alternating direction method of multipliers into a series of easy-to-solve shortest path subproblems. Each subproblem is then efficiently solved using a dynamic programming algorithm. Finally, the Xi'an–Chengdu high-speed railway line is used to test our model and algorithms, thereby demonstrating the trade-off between passenger-service quality and energy efficiency.

1. Introduction

High-speed railways have rapidly expanded around the world in recent decades, especially in China. By the end of 2020, the total length of China's high-speed railway network exceeded 36,000 km. High-speed train operations are generally based on an official timetable that stipulates the exact arrival and departure times for a train at a given station. However, real-time train operations are often affected by unexpected disruptions or disturbances (Cacchiani et al., 2014; Xu et al., 2016). Thus, conflicts may occur when two or more trains need to occupy the same piece of infrastructure simultaneously. In such situations, real-time dispatching/rescheduling is required to solve these conflicts and restore the original timetable. Here, *disruptions* are relatively large incidents that mandate significant changes to the timetable (i.e., re-timing, re-ordering, re-routing, or short-turning trains, or canceling services), and possibly to duties for rolling stock and crew (Cacchiani et al., 2014). In contrast, *disturbances* are relatively small occurrences that may be solved

* Corresponding authors.
E-mail addresses: shuguangzhan@my.swjtu.edu.cn (S. Zhan), pengling_wang@tongji.edu.cn (P. Wang).

https://doi.org/10.1016/j.tre.2021.102492
Received 11 March 2021; Received in revised form 30 August 2021; Accepted 18 September 2021
Available online 23 December 2021
1366-5545/© 2021 The Authors. Published by Elsevier Ltd. This is an open access article under the CC BY-NC-ND license (http://creativecommons.org/licenses/by-nc-nd/4.0/).

by slight modifications to the timetable (i.e., re-timing or re-ordering trains). In principle, adding more buffer time to the official timetable or making a more robust timetable can prevent the occurrence of certain disturbances or absorb small disturbances. However, the effect of disruptions usually cannot be eliminated by the addition of buffer time to the official timetable, making real-time rescheduling inevitable. Many researchers have investigated real-time timetable rescheduling in recent decades, and there are many comprehensive reviews on the algorithmic tools used for railway rescheduling (Cacchiani et al., 2014; Corman and Meng, 2015). The basic principle is to restore the original timetable by re-routing, re-timing, or re-ordering trains, or canceling services, while fulfilling objectives such as reducing the total or consecutive delay. However, energy efficiency has not been widely considered in these train rescheduling problems.

Although rail is one of the most environment-friendly modes of transport, the energy efficiency of train operations still lacks attentions from railway undertakings, even though improving energy efficiency can considerably reduce operation costs and enhance market positions. Among the various measures of energy-efficient railway operation, energy-efficient timetabling and energy-efficient train control have been widely investigated (Scheepmaker et al., 2017). In contrast, the energy-efficient train rescheduling problem has attracted little attention (Montrone et al., 2018). Logically, delayed trains should be driven as fast as possible to catch up with their schedules, but this strategy is rather energy-expensive and does not improve the energy efficiency of railway operations. Therefore, it is interesting to explore whether the need for the speeding up of trains can be reduced in cases of disturbances or disruptions by, for example, incorporating waiting times to allow for slow driving and reduce unexpected stops. More specifically, in the event of significant disruptions, the affected trains may need to stop at certain stations to wait until the disruption has been cleared. Thus, a disrupted train could be driven at fast speeds to recover time, but may then experience a long wait elsewhere until the disruption is resolved. Alternatively, a disrupted train could be driven slowly instead of stopping to wait for the disruption to be resolved. The former approach tends to consume more energy than the latter due to the increased speed of driving. Similarly, a disrupted train may have, for example, two 5-min unscheduled stops at two different places or a single 10-min unscheduled stop at one place. The delays in the two cases are the same, but the former would consume more energy than the latter as it involves more stops, which are typically energy-expensive. These two examples show the potential for energy saving in terms of disruptions. This paper aims to consider energy efficiency in the train rescheduling problem and investigate the trade-off between delay recovery and energy saving in the case of a large disruption.

1.1. Literature review

The energy efficiency of train operations has been widely studied in the train operation control and timetable planning phases. A well-designed timetable must include some running-time supplements to allow delayed trains to recover from small disturbances by driving fast; punctual trains can make use of these time supplements to drive slowly and save energy. Here, the running-time supplement refers to the running time beyond the technically minimum required time for running from one station to the next (Scheepmaker et al., 2017). The energy-efficient train operation problem often aims at optimizing train speed profiles to make better use of time supplements and energy. Energy-efficient timetabling, in contrast, deals with optimizing the amount and allocation of running-time supplements to improve the performance of energy-efficient driving (Sicre et al., 2010; Cucala et al., 2012; Scheepmaker et al., 2020).

Previous studies have shown that an energy-efficient driving strategy for a train running on flat tracks consists of maximum acceleration, cruising, coasting, and maximum braking (Howlett and Pudney, 2012; Albrecht et al., 2016a,b), whereas the optimal sequences and switching points of these driving regimes depend on speed limits, gradients, and running-time supplements. Various approaches, such as Pontryagin's maximum principle (Howlett and Pudney, 2012; Albrecht et al., 2016a,b), nonlinear programming (Ye and Liu, 2017), and pseudospectral methods (Wang and Goverde, 2016), have been used to identify the optimal sequences and switching points of these driving regimes.

With respect to the energy-efficient timetabling problem of optimizing the amount and allocation of running-time supplements, Scheepmaker and Goverde (2015) developed an "Energie Zuinig Rijden" model (EZR, Dutch) to determine the most energy-efficient trajectory of an individual train trip. The EZR model has been adopted to analyze the energy efficiency of practical train movements and develop real-world timetables. When the model is used, the more uniform allocation of the running time supplements leads to extra energy savings and an improvement in punctuality relative to when the method of tightening the timetable is used. Goverde et al. (2016) proposed a three-level timetable design method, which constructs a stable robust conflict-free timetable with optimal train orders first and then adjusts time supplements between the stops of regional trains in a corridor between two main stations for energy efficiency. The time supplements are re-allocated to optimize the energy-saving train operations and take stochastic dwell times into account. The problem is formulated as a multi-stage, multi-criteria decision problem that is solved by dynamic programming (DP). Canca and Zarzo (2017) studied the energy-efficient timetabling problem in rapid railway transit networks. The timetable design problem is formulated as a mixed integer nonlinear programming model, and the train energy consumption is described as a function of running times. Both are solved using a sequential mixed integer linear solving process.

The above studies separately address the energy-efficient train operation and energy-efficient timetabling problems. However, the railway timetable and train driving strategies are closely related to the energy costs of train operations. Recent studies have paid more attention to the integrated optimization of timetabling and train operation for energy efficiency. For instance, Li and Lo (2014), Liu et al. (2018), and Li et al. (2020) applied a nonlinear programming model to formulate the integrated problem and solved it using a genetic algorithm. Wang and Goverde (2019) proposed an energy-efficient timetable-adjustment method that relaxes the original arrival and departure times into time windows, and then used a pseudospectral method to adjust the arrival/departure times within these time windows to save the energy costs of railway operation. The long computational time of this method is suitable for small-scale cases, but not for large-scale cases. Xu et al. (2020) formulated energy-efficient train timetabling with a nonlinear programming model and transferred it into an integer linear programming (ILP) model based on a space–time–speed (STS) hypernetwork. They suggested that the optimization of an energy-efficient speed profile can be performed offline in advance to reduce the required computational time.

Compared with energy-efficient timetabling, the energy-efficient train rescheduling problem has received considerably less attention. Disruptions in daily train operations may occur due to bad weather, breakdown of the tracks or rolling stock, human error, and other factors. These disruptions can cause trains to deviate from the official timetables and require real-time dispatching or rescheduling to resolve conflicts and restore the original timetable. Cacchiani et al. (2014), Corman and Meng (2015), and Fang et al. (2015) reviewed a wide range of studies on train rescheduling from the perspectives of problems, models, algorithms, and case studies. This paper reviews only the most closely related studies on train rescheduling in the context of a major disruption. Louwerse and Huisman (2014) and Veelenturf et al. (2016) investigated the train rescheduling problem when a segment between two stations is partially or completely blocked on a Dutch railway corridor or network, respectively. They aimed to minimize both the train delay and train cancelations in a scenario where the trains can only perform a short-turn at the stations closest to the blocked location. Ghaemi et al. (2018) allowed trains to short-turn at multiple stations in the event of a complete blockage and developed a mixed ILP (MILP) model to determine the best strategy that would allow trains to short-turn. Zhu and Goverde (2019) further extended the flexibility of short-turning by permitting it at every possible station. Zhan et al. (2015) focused on the train rescheduling problem for high-speed lines in China, where trains cannot short-turn due to the use of a seat-reservation system. A waiting strategy was proposed to reschedule trains in terms of complete blockages. In this strategy, disrupted trains are required to stop and wait somewhere until the disruption is resolved. This work was extended in Zhan et al. (2016), in which they compared various train rescheduling strategies when one of the double tracks of a segment is blocked on a high-speed railway line. The objectives of these studies were to minimize train delays and cancelations, but not to optimize the energy efficiency. Zhan et al. (2015) formulated the train rescheduling problem in the context of a major disruption using an MILP model, in which many big "M" constraints were applied to model the "if-then" condition. However, they did not take energy consumption into account. The current study formulates the train rescheduling problem using an STS network-based model, in which the big "M" constraints are eliminated. Thus, the new model can be more easily decomposed into single-train rescheduling subproblems, allowing one to embed the energy efficiency factor.

Recent studies on the energy-efficient rescheduling problem have some limitations. Wang and Goverde (2017) used a pseudo-spectral method to reschedule trains after short delays on a single-track railway line, thereby minimizing delays and energy consumption. Similarly, Yang et al. (2019b) used an ILP model to reschedule metro trains after delay perturbations to minimize delays and energy consumption. Metro train rescheduling after short delays has also been addressed using deep learning (Kuppusamy et al., 2020) and reinforcement learning (Yang et al., 2019a). However, to the best of our knowledge, energy-efficient train rescheduling during a major disruption in which some tracks are completely blocked for relatively long periods of time (e.g., 90 min) has not been investigated. The scenario addressed in the current study differs from the small delays addressed in previous studies in two ways. First, some trains must stop at certain stations and wait for the disruption to end. Second, the train deviation cannot be eliminated in a short time, as can be done in a small delay situation.

Given the background information and literature review, we notice some knowledge gaps:

- To the best of our knowledge, energy-efficient train rescheduling during a major disruption (e.g., a track blockage) has not been investigated. Different from energy-efficient train rescheduling in a minor disruption scenario, energy-efficient train rescheduling during a major disruption needs to determine the stopping pattern (i.e., unscheduled stop times and locations) of disrupted trains and requires to reschedule a larger number of trains, which will complicate the modeling and solution procedure of the problem.
- The railway timetable and train driving strategies closely influence the energy costs of train operations. Therefore, it is necessary to take both factors into account. However, such an integration increases the complexity of the problem and may require long computational times that are not suitable to real-time scheduling. Given this limitation, a powerful solution is required.

1.2. Focus of this study

This study focuses on real-time high-speed train rescheduling in the face of a major disruption, and attempts to reduce the total train delay and energy consumption. This paper proposes a two-level energy-efficient rescheduling approach: in the first level, a

microscopic train trajectory optimization method is used to compute train speed curves and energy costs; in the second level, a macroscopic train rescheduling method is introduced to optimize real-time arrival and departure times to save energy and increase delay recovery.

More specifically, this study focuses on rescheduling trains on a double-track high-speed rail corridor during a major disruption that involves the complete blockage of some track sections (segments) for a relatively long time (e.g., 90 min). The trains cannot go through the disrupted tracks and, due to the seat reservation system, cannot short-turn. Therefore, the trains must wait somewhere until the disruption is resolved (Zhan et al., 2015). We seek to build an energy-efficient train scheduling method. To achieve this, we first specify all possible train runs; a train run is a train movement between two adjacent stations with a given departure time and speed and a given arrival time and speed. We then compute the optimal speed–distance curves and corresponding energy costs of all possible train runs using a multiple-phase optimal train control model and a pseudospectral method. The multiple-phase optimal train control model accounts for detailed environmental (line speed limits, gradients, and curves) and dynamic (specific deceleration and acceleration rates) characteristics of trains. The speed profile optimization method was first proposed by Wang and Goverde (2016) to compute the speed profile between two stops (with departure and arrival speeds set to zero). This study extends the method to optimize the speed profiles with any given departure and arrival speeds. Notably, the speed profile optimization is performed offline in advance, and the solutions (the set of potential speed profiles) are used as inputs to the macroscopic rescheduling model, substantially reducing the computational burden (Xu et al., 2020).

At the second level, i.e., in the macroscopic rescheduling model, we introduce an STS hypernetwork (Zhou et al., 2017) for train rescheduling. An ILP model is formulated for the macroscopic train rescheduling problem. The ILP model selects the most appropriate speed profiles, i.e., those that minimize train delay and energy consumption, from the potential speed profile set that is computed offline. In addition, the macroscopic train rescheduling model is decomposed by the alternating direction method of multipliers (ADMM) into several easy-to-solve subproblems, with one subproblem for each train. Each subproblem is a shortest-path searching problem that is easily solved using an algorithm such as label correcting or DP. Our models and algorithms are tested on the Xi'an–Chengdu high-speed railway line. The test results demonstrate the efficiency of our proposed energy-efficient train rescheduling method.

To summarize, this study contributes to the energy-efficient rescheduling literature in the following three aspects:

- We use the STS hypernetwork for the first time for train rescheduling during a major disruption, in which the macroscopic train rescheduling problem and microscopic train speed profile optimizing problem are combined via the speed dimension. Our STS network for train scheduling differs from that presented by Zhou et al. (2017), as it considers different running times for a train in a given segment.
- We investigate the trade-off between energy saving and delay recovery for train rescheduling after a major disruption, which could help railway dispatchers choose the most appropriate dispatching strategy.
- By introducing the STS network, we model the energy-efficient train rescheduling problem using an ILP model. The complicated integrated problem is rapidly solved using the ADMM algorithm.

The remainder of this paper is organized as follows. In Section 2, model formulations are described for the macroscopic train rescheduling problem and microscopic train control problem. In Section 3, we present the decomposition of the train rescheduling model through the ADMM approach. Section 4 reports the computational results obtained from testing our models and algorithms on the Xi'an–Chengdu high-speed railway line. Finally, we conclude the study and discuss some future research directions in Section 5.

2. Model formulation

The train rescheduling problem primarily determines the times that a train arrives at and departs from a station during a disruption, and is usually formulated at the macroscopic level as an integer or MILP model (Meng and Zhou, 2014; Zhan et al., 2015, 2016; Veelenturf et al., 2016). However, energy-efficient train control is usually formulated in a nonlinear form. Optimal train speed control has been widely investigated and the optimal energy-efficient train speed profile in a segment between two consecutive stations is determined by the arriving and leaving speeds and the train's running time in the segment. Thus, we manage the energy-efficient train rescheduling problem from a macroscopic perspective by determining the arrival and departure times of trains at stations as well as the arriving and leaving speeds of trains in each segment. Therefore, the space–time network that is generally used in train scheduling/rescheduling is expanded to an STS network to account for train speed. We optimize the detailed train speed profile with a multiple-phase optimal control model for each segment between two consecutive stations, which considers the detailed characteristics of lines and trains and can be embedded into the macroscopic train rescheduling problem.

2.1. Notations and assumptions

The notations used in the model are given in Table 1.

Table 1
Notation used in the model.

Type	Notation	Description
Sets	T	Set of discrete times of the planning horizon
	K	Set of trains
	N	Set of railway network nodes
	V	Set of discrete train speeds
	L	Set of physical links connecting two physical nodes
	L_k	Set of physical links available to train $k \in K$, $L_k \subset L$
	A	Set of space–time–speed arcs
	A_k	Set of space–time–speed arcs available to train $k \in K$, $A_k \subset A$
	E	Set of space–time–speed nodes
	S	Set of stations, $S \subset N$
	$\overline{A}$	Set of space–time arcs
Indices	t, t', τ, τ'	Index of time, $t, t', \tau, \tau' \in T$
	k, k'	Index of trains, $k, k' \in K$
	$i, j(i,j)$	Index of physical nodes, $i, j \in N$ Index of physical links, $(i,j) \in L$
	u, u'	Index of train speeds, $u, u' \in V$
	$(i,t,u);(j,t',u')$	Index of space–time–speed nodes, $(i,t,u),(j,t',u') \in E$
	(i,t,u,j,t',u')	Index of space–time–speed arcs, $(i,t,u,j,t',u') \in A$
	(i,t,j,t')	Index of space–time arcs, $(i,t,j,t') \in \overline{A}$
Parameter	o_k	Origin of train k
	d_k	Destination of train k
	e_k	Earliest time of train k leaving its origin
	l_k	Latest time of train k arriving at its destination
	$\psi(i,t,j,t')$	Incompatible arc set of link (i,j) starting at t and ending at t'
	$c^k_{itujt'u'}$	Delay cost of train k taking arc $(i,t,u,j,t',u') \in A$
	$\overline{c}^k_{itujt'u'}$	Energy cost of train k using arc $(i,t,u,j,t',u') \in A$
	C_i	Capacity of station $i \in S$ (number of tracks)
	dw_i	Minimum dwell time at a scheduled-stop station $i \in S$ for trains
	$arr_{k,i}$	Scheduled time of train k arriving at station $i \in S$
	$dep_{k,i}$	Scheduled time of train k departing from station $i \in S$
	ω_1, ω_2	Weights of delay cost and energy consumption cost, respectively
Variables	$x^k_{i,t,u,j,t',u'}$	If train k uses arc (i,t,u,j,t',u'), then $x^k_{i,t,u,j,t',u'} = 1$; otherwise, $x^k_{i,t,u,j,t',u'} = 0$

The assumptions used in this study are as follows: (1) the tracks in a segment or a station on a double-track railway line are used separately by inbound and outbound trains, such that we can reschedule trains in each direction independently; (2) the occurrence time and end time of the disruption are known; (3) if two trains have sufficient headway at the start and end stations of a segment without overtaking, they do not conflict with each other within the segment; (4) we consider only the energy consumption needed to provide traction force, and not the energy generated by regenerative braking.

2.2. STS network

In an STS network, time is discretized into time intervals of δ, and the time horizon can be denoted as $T = \{\delta, 2\delta, 3\delta, \ldots \Theta\delta\}$, where Θ is the maximum number of time intervals. Each station i is regarded as a physical node, $i \in S \subset N$. N includes not only the station nodes, but also the origin and destination nodes (o_k and d_k) of each train k. To embed the train speed within the network, we add a speed dimension, in which the possible train speed is discretized into speed intervals of σ and the potential train speed set $V = \{\sigma, 2\sigma, 3\sigma, \ldots \kappa\sigma\}$, where κ is the maximum number of speed intervals. Because various train speed profiles are loaded in the actual high-speed train driving advisory system, it is reasonable to discretize the train speed into specific speed levels. Accordingly, a physical node $i \in N$ is expanded into an STS node $(i,t,u) \in E$, and a physical link $(i,j) \in L$ is expanded into an STS arc $(i,t,u,j,t',u') \in A$, which implies that a train leaving node i at time t with speed u would arrive at node j at time t' with speed u'. A physical link (i,j) can be a segment ($i \neq j$) or a station waiting link ($i = j$). Thus, the STS network is denoted as a graph $G = (E, A)$, where E is the STS node set and A is the STS arc set.

A train uses various types of arcs on the constructed STS graph G during its journey. Note that there is a dwell arc, to denote the planned dwell process at a station, and a stopping arc, to denote the extra stop at a station due to the disruption. We assume that trains have the same minimum dwell time at a planned dwell station, and that if a train has a longer planned dwell time at the station, it uses

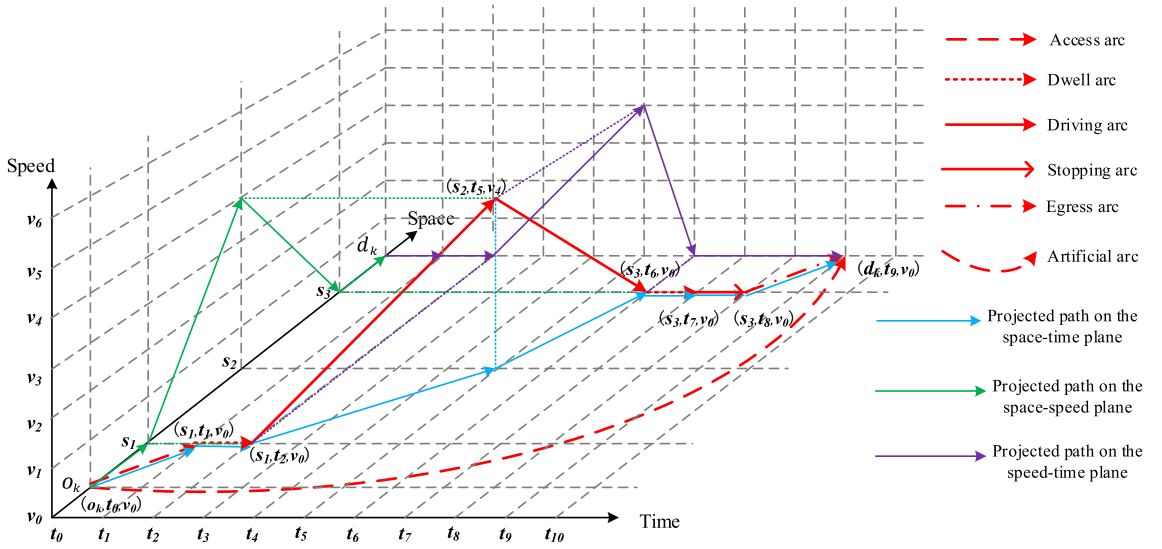

Fig. 1. Example of space–time–speed (STS) network.

additional stopping arcs. Therefore, the minimum dwell time required by a train at a station is captured by the dwell arc. These arcs are defined as follows, and a small-scale example of one train running on a line with three stations is given in Fig. 1 to help explain the STS network and various types of arcs.

- A driving arc $((i,t,u,j,t',u') \in A_{drive} \subset A)$ represents a train departing from node $(i,t,u) \in E$ at station i and time t with speed u and arriving at node $(j,t',u') \in E$ at the next station j at time t' with speed u'. The duration $(t'-t)$ of arc (i,t,u,j,t',u') is the running time of the train in the segment. As a train has various speed levels, its running time in a segment can have various values. A driving arc has a delay cost $c^k_{itujt'u'}$ and an energy cost $\bar{c}^k_{itujt'u'}$.
- A dwell arc $((i,t,u,j,t',u') \in A)$ represents a train with a scheduled dwell process at an intermediate station $i \in S$ from time t to time t', where $i=j$ and $u=u'=0$ for a dwell arc. The arc duration $(t'-t) = dw_i$. A dwell arc has no delay cost and the traction energy cost is assumed to be zero.
- A stopping arc $((i,t,u,j,t',u') \in A)$ represents a train with an unscheduled or extra dwell process at a station $i \in S$ (or its origin o_k or its destination d_k) from time t to time t', where $i=j$ and $u=u'=0$. This arc is defined as a unit arc, where $(t'-t)=\delta$. In this study, $\delta = 1$ min. If a train stops temporarily at a station (or at its origin or destination) for several minutes, we use several consecutive stopping arcs to represent the entire stopping process. Both the delay cost and traction energy cost for a stopping arc are assumed to be zero.
- An access arc $((o_k,t,0,j,t',0) \in A)$ represents a train k leaving from its origin and traveling to its first station. Thus, an access arc is used to connect an assumed train origin with the first station that it uses in the railway network. We therefore assume that both the delay cost and energy cost are zero.
- An egress arc $((j,t',0,d_k,t,0) \in A)$ represents a train k leaving its final station and arriving at the destination. Like the access arc, both its delay cost and energy cost are zero.
- An artificial arc $((o_k,e_k,0,d_k,l_k,0) \in A)$ represents a train k that starts from its origin o_k at time e_k and ends at its destination d_k at time l_k, which is defined to manage train cancelation. If a train is canceled due to the disruption, we assume that it uses an artificial arc to finish its journey. An artificial arc has no corresponding delay or energy costs, but a large penalty is given for a cancelation.

To model the train rescheduling process, the constructed STS network must adhere to the following principles:

- The duration of a driving arc between two consecutive stations must not be shorter than the minimum running time. In addition, if a train is scheduled to stop at a station, it must use one and only one dwell arc at this station. Therefore, the minimum running time and dwell time constraint for a train can be embedded within the STS network at the network-construction stage. Detailed information on how to assign a dwell arc to a train at a planned stop station is given in Appendix A.
- If a disruption forces a train to stop at a station for longer than the scheduled time, it uses several stopping arcs. Note that we do not stipulate a maximum extra stopping time for a train because this depends on the disruption scenario, and it is not easy to select a value that ensures feasibility of the solution.
- If a disruption results in a train being canceled, then the train uses an artificial arc to finish its trip.
- If a disruption results in some arcs being unavailable, then these arcs are deleted from the STS network.

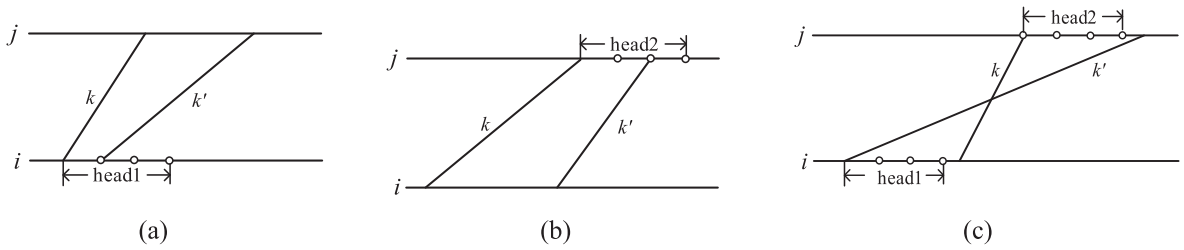

Fig. 2. Examples of incompatible arcs due to (a) departure headway incompatibility, (b) arrival headway incompatibility, and (c) overtaking.

- The train speed within a constructed STS arc must be within the allowable speed range, as this will reduce the number of arcs. For example, if a train must stop at a station, then both the arrival and departure speeds at that station must be zero.

2.3. Detailed model formulation

In this subsection, we first introduce the ILP model used for the macroscopic train rescheduling problem, and then the multiple-phase optimal control model used for the microscopic train speed profile optimization problem.

2.3.1. Train rescheduling model (*M*)

We aim to minimize both the train delay from the passengers' perspective and energy consumption from the train operators' perspective. Therefore, the objective function is represented as follows:

$$\textbf{Min}: \quad \omega_1 \times \left(\sum_{k\in K} \sum_{(i,t,u,j,t',u')\in A_k} c^k_{itujt'u'} \times x^k_{i,t,u,j,t',u'} \right) + \omega_2 \times \left(\sum_{k\in K} \sum_{(i,t,u,j,t',u')\in A_k} \overline{c}^k_{itujt'u'} \times x^k_{i,t,u,j,t',u'} \right) \tag{1}$$

In objective (1), the first sum calculates the total train arrival deviation cost, and the second sum calculates the total energy consumption of the train operations. We consider only the train arrival deviation (earliness and tardiness) for a driving arc (i,t,u,j,t',u'), $c^k_{itujt'u'} = \max\{t' - arr_{kj}, arr_{kj} - t'\}$, and do not consider the departure deviation. However, it is easy to extend the train arrival deviation to other objectives. The parameters ω_1 and ω_2 are the weights for the total train arrival deviation cost and total energy consumption of train operations, and their values can be selected by railway managers. To simplify the notation, the cancelation penalty is denoted by $c^k_{itujt'u'}$ for the artificial arc (i,t,u,j,t',u').

Subject to:

1) Train flow conservation constraints:

$$\sum_{(j,t',u')\in A_k} x^k_{i,t,u,j,t',u'} - \sum_{(j,t',u')\in A_k} x^k_{j,t',u',i,t,u} = \begin{cases} 1 & i = o_k, t = e_k, u = 0 \\ -1 & i = d_k, t = l_k, u = 0 \\ 0 & otherwise \end{cases} \quad \forall k \in K \tag{2}$$

2) Headway constraint:

$$\sum_{k'\in K} \sum_{(i,t,u,j,t',u')\in A_{k'}} x^{k'}_{i,t,u,j,t',u'} + \sum_{(i,\tau,u,j,\tau',u')\in \psi(i,t,j,t')} x^k_{i,\tau,u,j,\tau',u'} \le 1 \quad \forall (i,t,j,t') \in \overline{A} : i \ne j, \quad \forall k \in K \tag{3}$$

3) Station capacity constraint:

$$\sum_{k\in K} \sum_{\tau\in T} \sum_{(i,\tau,0,i,t',0)\in A_k} x^k_{i,\tau,0,i,t',0} + \sum_{k\in K} \sum_{(i,t,u,j,t',u')\in A_k} x^k_{i,t,u,j,t',u'} \le C_i \quad \forall i \in S : j = i+1, \forall t \in T \tag{4}$$

where $\tau = t$ if $(i,\tau,0,i,t',0) \in A_k$ is a stopping arc, and $t - dw_i < \tau \le t$ if $(i,\tau,0,i,t',0) \in A_k$ is a dwell arc.

4) Train departure constraint:

$$x^k_{i,t,u,j,t',u'} = 0 \quad \forall k \in K, \quad \forall (i,t,u,j,t',u') \in A_{drive} \cap A_k : t < dep_{k,i} \tag{5}$$

5) The domain of train scheduling variable $x^k_{i,t,u,j,t',u'}$ is shown in constraint (6).

$$x^k_{i,t,u,j,t',u'} \in \{0,1\} \; \forall k \in K, \forall (i,t,u,j,t',u') \in A_k \tag{6}$$

Constraint (2) is a flow conservation constraint that ensures that a train runs from its origin to its destination. Constraint (3) ensures that the minimum headway between any two trains in a given segment is met; this prevents the overtaking of one train by another in the segment, and is achieved by defining the incompatible arc set $\psi(i,t,j,t')$. The first sum of constraint (3) counts the number of trains that use arcs belonging to $(i,t,j,t') \in \overline{A}$, where $(i,t,j,t') \in \overline{A}$ includes all STS arcs (i,t,u,j,t',u'); the second sum determines whether train k uses any arc that belongs to the incompatible arc set $\psi(i,t,j,t')$. Constraint (3) stipulates that if a train uses the space–time arc (i,t,j,t'), then no other train is allowed to use STS arcs incompatible with this arc. Some studies have used this incompatible set to

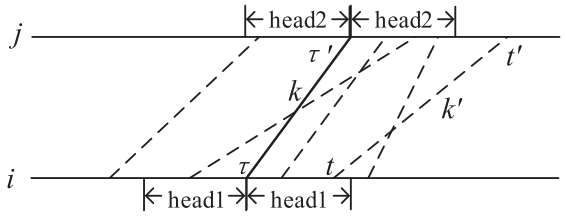

Fig. 3. Example of an incompatible arc set.

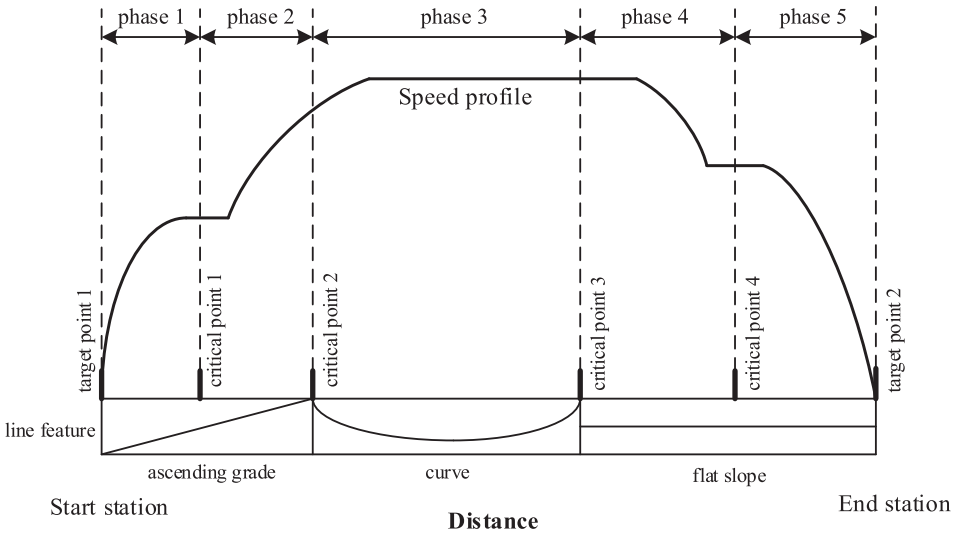

Fig. 4. Example of multiple-phase division of a segment between two stations.

model the headway, similar to the clique set defined, for example, by Caprara et al. (2002). The incompatible arcs are explained in a later section of this paper. The station capacity constraint is given by inequality (4); this is very important in train rescheduling, but is not normally considered in train timetabling. The station capacity constraint states that for each station $i \in S$ and at any time $t \in T$, the total number of trains that dwell ($\sum_{k\in K}\sum_{\tau\in T}\sum_{(i,\tau,0,i,\tau+dw_i,0)\in A_k} x^k_{i,\tau,0,i,\tau+dw_i,0}$) or stop ($\sum_{k\in K}\sum_{(i,t,0,i,t+\delta,0)\in A_k} x^k_{i,t,0,i,t+\delta,0}$) at the station and pass the station ($\sum_{k\in K}\sum_{(i,t,u,j,t',u')\in A_k} x^k_{i,t,u,j,t',u'}$) cannot be larger than the station capacity. Constraint (4) stipulates that if $(i,\tau,0,i,t',0) \in A_k$ is a dwell arc, then all dwell arcs in which $t - dw_i < \tau \le t$ must be counted because a dwell arc is not a unit arc and a dwell may last for several minutes. For example, if a train starts to dwell at station i at time t, and this dwell lasts for 2 min (i.e., dw_i is 2 min), then the train occupies the station at time t and at time $t+1$. Therefore, we must count all of the trains that dwell at a given station at a certain time, rather than counting only the dwell arcs that begin at that time. Note that if a train does not stop at, but passes station i, then the departure arc is sufficient to indicate whether the train has used a track at that station. Therefore, it is not necessary to calculate the number of arriving trains in constraint (4). Constraint (5) stipulates that a train does not depart from a station before its scheduled departure time, ensuring that passengers do not miss their scheduled trains. Constraint (6) represents the domain of variable $x^k_{i,t,u,j,t',u'}$. Finally, because the timetable has been partly implemented by the time a disruption occurs, we incorporate the schedule before the occurrence of the disruption based on the official timetable into the above model for our rescheduling problem.

Examples of incompatible arc sets for various types of headways are shown in Fig. 2. In Fig. 2 (a), (b), and (c), nodes i and j are two end stations of a segment. Fig. 2(a) shows that trains k and k' are incompatible because the departure headway is shorter than the minimum departure headway (head1); Fig. 2(b) shows that trains k and k' are incompatible because the arrival headway is shorter than the minimum arrival headway (head2); Fig. 2(c) shows that although the departure and arrival headways of trains k and k' are ensured, these two trains are still incompatible because they overtake each other within the segment. As we allow trains to run at different speeds within a segment, overtaking is possible. For each driving arc between stations i and j departing at time τ and arriving at time τ' (shown by the solid line in Fig. 3), the corresponding incompatible arc set $\psi(i,\tau,j,\tau')$ includes all of the driving arcs (shown by the dotted lines in Fig. 3). The incompatible arc set for any incompatible driving arc between stations i and j departing at time t and arriving at time t' is represented by Equation (3a), as follows:

$$\psi(i,\tau,j,\tau') = \{(i,t,u,j,t',u') \in A_{drive} | \tau - h_{k'k} < t < \tau + h_{kk'}\} \tag{3a}$$

where $h_{k'k}$ is the departure headway required between trains k' and k when k' departs before k. Parameter $h_{k'k}$ is defined as $h_{k'k} =$

$\max\{head1, [(t^{'} - t) - (\tau^{'} - \tau) + head1]\}$. Here $(t^{'} - t)$ and $(\tau^{'} - \tau)$ are the running times of the two driving arcs. Similarly, $h_{kk^{'}}$ is the departure headway required between trains k and $k^{'}$ when $k^{'}$ departs after k. Parameter $h_{kk^{'}}$ is defined as $h_{kk^{'}} = \max\{head1, [(\tau^{'} - \tau) - (t^{'} - t) + head1]\}$. If an arc corresponding to $(i, \tau, j, \tau^{'})$ is occupied, then no train can use any arc in $\psi(i, \tau, j, \tau^{'})$.

2.3.2. Single-train trajectory optimization on a link between two consecutive stations

The macroscopic train rescheduling model presented above uses the energy cost of each driving arc as an input. The energy costs are computed offline via a multiple-phase train trajectory optimization approach. This approach has been applied in previous studies, as in Wang and Goverde (2016; 2017), and is used here to optimize the train movement and calculate the energy cost of each driving arc.

In our train trajectory optimization problem, the train is treated as a point of mass m. Distance s is the independent variable, and train speed v and time t are the dependent variables, denoted by $v(s)$ and $t(s)$, respectively. To account for the detailed features of tracks (speed limits, gradients, and curves), the train trajectory planning problem is formulated as a multiple-phase optimization problem, in which a link between two stations is further divided into several phases by target points (the start and end stations of a driving arc) and critical points (speed limit and curve or gradient change points). Thus, the speed limit, curve, and gradient remain constant within each phase. The example in Fig. 4 demonstrates how a train journey between two stations is divided into multiple phases. In the figure, critical points 1 and 4 are speed limit points, and critical points 2 and 3 are curve or gradient change points. The segment is divided into five phases by these six points. Therefore, we can optimize the train trajectory in each phase and combine the resulting optimized trajectories by linking the constraints between adjacent phases.

It is assumed that a driving link (i,j) between stations i and j is divided into P phases. We use $\boldsymbol{P}$ to represent the phase set and p to represent a phase within $\boldsymbol{P}$. Based on the general optimal train control mode in Appendix B and the phase division above, the multiple-phase optimal control problem of a train $k \in K_p$ on a link is formulated as follows (K_p is the train set comprising trains in phase p, and the other notation is defined in Table 2 in the Appendix B):

$$\min \quad \sum_{p\in \boldsymbol{P}} \int_{s_0^{(p)}}^{s_f^{(p)}} f_k^{(p)}(s) ds, \tag{15}$$

subject to

1) The following dynamic constraints:

$$\begin{cases} \dfrac{dv_k^{(p)}(s)}{ds} = \dfrac{\theta_1 f_k^{(p)}(s) - \theta_2 b_k^{(p)}(s) - R_{train}\left(v_k^{(p)}\right) - R_{line}^{(p)}(s)}{\varepsilon \cdot m \cdot v_k^{(p)}(s)} \\ \dfrac{dt_k^{(p)}(s)}{ds} = \dfrac{1}{v_k^{(p)}(s)} \end{cases} \quad \forall p \in \boldsymbol{P}, \forall k \in K_p. \tag{16}$$

2) The following path constraints:

$$\begin{cases} 0 \le f_k^{(p)}(s) \le F_{max} \\ 0 \le b_k^{(p)}(s) \le B_{max} \\ 0 \le f_k^{(p)}(s) \cdot v_k^{(p)}(s) \le P_{max} \\ 0 \le v_k^{(p)}(s) \le V_{max}^{(p)}(s) \\ A_{min} \le \dfrac{dv_k^{(p)}(s)}{dt_k^{(p)}(s)} \le A_{max} \end{cases} \quad \forall p \in \boldsymbol{P}, \forall k \in K_p \tag{17}$$

3) The following coordination constraints for the first and last phases of a link between two consecutive stations:

$$\begin{cases} v_k^{(1)}\left(s_0^{(1)}\right) = \overline{u}, \\ v_k^{(P)}\left(s_f^{(P)}\right) = \overline{u^{'}}, \\ t_k^{(1)}\left(s_0^{(1)}\right) = \overline{t}, \\ t_k^{(P)}\left(s_f^{(P)}\right) = \overline{t^{'}}, \end{cases} \quad \forall k \in K_p. \tag{18}$$

4) The following linkage constraint between two consecutive phases:

$$\begin{cases} v_k^{(p)}\left(s_f^{(p)}\right) = v_k^{(p+1)}\left(s_0^{(p+1)}\right) \\ t_k^{(p)}\left(s_f^{(p)}\right) = t_k^{(p+1)}\left(s_0^{(p+1)}\right) \end{cases} \quad \forall p \in \boldsymbol{P} : p+1 \le P, \forall k \in K_p. \tag{19}$$

In the multiple-phase train control model, objective (15) minimizes the total traction energy cost of train k in all of the phases on a link. This energy consumption corresponds to the energy cost of $\overline{c}^{k}_{ituijt'u'}$ in the macroscopic train rescheduling problem. The dynamic constraints (16) are the dynamic differential equations for each train in each phase. The path constraints (17) stipulate that the vehicle characteristics (maximum traction force, braking force, and power) must be accounted for and that passenger comfort and the speed limit must be ensured. The coordination constraints (18) ensure that the start time and speed at the origin station and the end time and speed at the destination station of a link must remain the same as the values given by the train rescheduling model (arc $(i,\overline{t},\overline{u},j,\overline{t'},\overline{u'})$). Here, arc $(i,\overline{t},\overline{u},j,\overline{t'},\overline{u'})$ is that used by train k on the link (i,j). The linkage constraints (19) connect the states of consecutive phases.

The multiple-phase single-train control model is solved using pseudospectral methods, in which the continuous optimal-control model is discretized into a nonlinear programming model. This model is solved using a nonlinear software package in MATLAB. Detailed information about the pseudospectral method can be found in Wang et al. (2015).

3. Solution algorithm for the macroscopic train rescheduling model

The train rescheduling model in Section 2.3.1 is an ILP model, small-scale cases of which can be directly solved using CPLEX. However, a real-world case may be difficult to solve, as too many variables may exist in the corresponding space–time-based ILP model. In such cases, a decomposition approach is used to decompose the ILP model and thus reduce the computational burden. Lagrangian relaxation (LR) is typically used to relax the complex constraints of a model to make it decomposable. However, because LR reduces the ease of finding a feasible solution for the primal problem, the ADMM (Boyd et al., 2011) is used to decompose our model.

As the headway constraint (3) and station capacity constraint (4) correspond to many trains and not a single train, we relax these two constraints. We introduce a quadratic penalty parameter ρ_1 and Lagrange multiplier $\mu^{k}_{i,\tau,j,\tau'}$ for constraint (3), and a quadratic penalty parameter ρ_2 and Lagrange multiplier π^{t}_{i} for constraint (4). The ILP model in Section 2.3.1 is relaxed as follows ($\mathbf{M}_{\mathrm{ADMM}}$):

Min:

$$
\begin{aligned}
&\omega_1 \times \left(\sum_{k\in K} \sum_{(i,t,u,j,t',u')\in A_k} c^{k}_{ituijt'u'} \times x^{k}_{i,t,u,j,t',u'} \right) + \omega_2 \times \left(\sum_{k\in K} \sum_{(i,t,u,j,t',u')\in A_k} \overline{c}^{k}_{ituijt'u'} \times x^{k}_{i,t,u,j,t',u'} \right) + \sum_{(i,t,j,t')} \sum_{k\in K} \mu^{k}_{i,t,j,t'} \left(\sum_{k'\in K} \sum_{(i,t,u,j,t',u')\in A_{k'}} x^{k'}_{i,t,u,j,t',u'} \right. \\
&\left. + \sum_{(i,\tau,u,j,\tau',u')\in \psi(i,t,j,t')} x^{k}_{i,\tau,u,j,\tau',u'} - 1 \right) + \\
&\frac{\rho_1}{2} \sum_{(i,t,j,t')} \sum_{k\in K} \left\| \sum_{k'\in K} \sum_{(i,t,u,j,t',u')\in A_{k'}} x^{k'}_{i,t,u,j,t',u'} + \sum_{(i,\tau,u,j,\tau',u')\in \psi(i,t,j,t')} x^{k}_{i,\tau,u,j,\tau',u'} - 1 \right\|_2^2 + \\
&\sum_{i\in S} \sum_{t\in T} \pi^{t}_{i} \left(\sum_{k\in K} \sum_{\tau\in T} \sum_{(i,\tau,0,i,t',0)\in A_k} x^{k}_{i,\tau,0,i,t',0} + \sum_{k\in K} \sum_{(i,t,u,j,t',u')\in A_k} x^{k}_{i,t,u,j,t',u'} - C_i \right) + \\
&\frac{\rho_2}{2} \sum_{i\in S} \sum_{t\in T} \left\| \sum_{k\in K} \sum_{\tau\in T} \sum_{(i,\tau,0,i,t',0)\in A_k} x^{k}_{i,\tau,0,i,t',0} + \sum_{k\in K} \sum_{(i,t,u,j,t',u')\in A_k} x^{k}_{i,t,u,j,t',u'} - C_i \right\|_2^2
\end{aligned}
\tag{20}
$$

subject to (2) and (6).

The relaxed model is much simpler than the primal model as it has only a flow conservation constraint (2) and a variable domain constraint (6). Therefore, the constraints can be decomposed for each train. Note that the train departure constraint (5) can be embedded within the DP algorithm by adding a departure time window in the shortest-path searching process, which is explained in Appendix A. However, the objective function (20) has two quadratic terms $\|\bullet\|_2^2$ and is not directly decomposable. We use an ADMM procedure to successively solve the train rescheduling problem for each train via a block coordinate-descent method, i.e., when we reschedule one train, the schedules of the other trains are regarded as fixed. For example, in a scenario with two variables, x_1 and x_2, $(x_1 + x_2 - c)^2 = [x_1 + (x_2 - c)]^2 = {x_1}^2 + 2 \times x_1 \times (x_2 - c) + (x_2 - c)^2 = [2 \times (x_2 - c) + 1] \times x_1 + (x_2 - c)^2$, where ${x_1}^2 = x_1$ because x_1 is a binary variable, x_2 is fixed when we optimize x_1, and c is a parameter. Thus, the quadratic terms can be linearized. In addition, although ADMM is typically used to relax the equality constraints, it can also be used for inequality constraints. For inequality ("$\leq$") constraints (3) and (4), the first quadratic penalty term is only added when $\sum_{k'\in K}\sum_{(i,t,u,j,t',u')\in A_{k'}} x^{k'}_{i,t,u,j,t',u'} + \sum_{(i,\tau,u,j,\tau',u')\in \psi(i,t,j,t')} x^{k}_{i,\tau,u,j,\tau',u'} > 1$, and the second quadratic penalty term is only added when $\sum_{k\in K}\sum_{\tau\in T}\sum_{(i,\tau,0,i,t',0)\in A_k} x^{k}_{i,\tau,0,i,t',0} + \sum_{k\in K}\sum_{(i,t,u,j,t',u')\in A_k} x^{k}_{i,t,u,j,t',u'} > C_i$. In this way, the two inequality constraints can be handled by ADMM. For more detailed information on handling inequality constraints using ADMM, we refer the reader to Zhan et al. (2021).

After the relaxation of the model and linearization of the relaxed objective function, the primal model can be decomposed into easy-to-solve subproblems as follows, with one for each train ($\mathbf{M}^{k}_{\mathrm{ADMM}}$):

$$\min: Z_k = \omega_1 \times \left(\sum_{(i,t,u,j,t',u') \in A_k} c^k_{itujt'u'} \times x^k_{i,t,u,j,t',u'} \right) + \omega_2 \times \left(\sum_{(i,t,u,j,t',u') \in A_k} \overline{c}^k_{itujt'u'} \times x^k_{i,t,u,j,t',u'} \right) +$$
$$\sum_{(i,t,j,t')} \mu^k_{i,t,j,t'} \times \sum_{k' \in K} \sum_{(i,t,u,j,t',u') \in A_{k'}} x^{k'}_{i,t,u,j,t',u'} + \sum_{(i,t,j,t')} \mu^k_{i,t,j,t'} \sum_{(i,\tau,u,j,\tau',u') \in \psi(i,t,j,t')} x^k_{i,\tau,u,j,\tau',u'} + \frac{\rho_1}{2} \times \sum_{(i,t,j,t')} \left(2\vartheta^k_{i,t,j,t'} - 1 \right) \times x^k_{i,t,u,j,t',u'} +$$
$$\sum_{i \in S} \sum_{t \in T} \pi^t_i \times \left(\sum_{\tau \in T} \sum_{(i,\tau,0,i,t',0) \in A_k} x^k_{i,\tau,0,i,t',0} + \sum_{(i,t,u,j,t',u') \in A_k} x^k_{i,t,u,j,t',u'} \right) + \frac{\rho_2}{2} \times \sum_{i \in S} \sum_{t \in T} \left(2\varphi^k_{i,t} - 2C_i + 1 \right) \times x^k_{i,t,u,j,t',u'} = \widehat{c}^k_{itujt'u'} \times x^k_{i,t,u,j,t',u'} \quad (21)$$

subject to (2) and (6),

where the general cost coefficient is calculated by Equation (22), and the following property (Equation (21a)) holds in (21). The detailed proof of this property is given in Appendix C.

Property 1:. $\sum_{(i,t,j,t')} \mu^k_{i,t,j,t'} \sum_{(i,\tau,u,j,\tau',u') \in \psi(i,t,j,t')} x^k_{i,\tau,u,j,\tau',u'} = \sum_{(i,\tau,u,j,\tau',u') \in \psi(i,t,j,t')} \mu^k_{i,\tau,j,\tau'} \times \sum_{(i,t,u,j,t',u')} x^k_{i,t,u,j,t',u'}$ (21a)

In the following Equation (22), $(i,t,j,t') \in \overline{A} : i \neq j$ in constraint (3) is simplified by $(i,t,j,t') \in \overline{A}$, but we should keep in mind that link (i,j) here is a segment link between two stations i and j.

$$\widehat{c}^k_{itujt'u'} = \begin{cases} \omega_1 \times c^k_{itujt'u'} + \omega_2 \times \overline{c}^k_{itujt'u'} & if (i,t,j,t') \notin \overline{A} \text{ and } i \notin S \\ \omega_1 \times c^k_{itujt'u'} + \omega_2 \times \overline{c}^k_{itujt'u'} + \sum_{k' \in K} \mu^{k'}_{i,t,j,t'} + \sum_{(i,\tau,j,\tau') \in \psi(i,t,j,t')} \mu^k_{i,\tau,j,\tau'} + \frac{\rho_1}{2} \times \left(2\vartheta^k_{i,t,j,t'} - 1 \right) & \\ if (i,t,j,t') \in \overline{A} \text{ and } i \notin S & \\ \omega_1 \times c^k_{itujt'u'} + \omega_2 \times \overline{c}^k_{itujt'u'} + \pi^t_i + \frac{\rho_2}{2} \times \left(2\varphi^k_{i,t} - 2C_i + 1 \right) & if (i,t,j,t') \notin \overline{A} \text{ and } i \in S \\ \omega_1 \times c^k_{itujt'u'} + \omega_2 \times \overline{c}^k_{itujt'u'} + \sum_{k' \in K} \mu^{k'}_{i,t,j,t'} + \sum_{(i,\tau,j,\tau') \in \psi(i,t,j,t')} \mu^k_{i,\tau,j,\tau'} + \frac{\rho_1}{2} \times \left(2\vartheta^k_{i,t,j,t'} - 1 \right) + & \\ \pi^t_i + \frac{\rho_2}{2} \times \left(2\varphi^k_{i,t} - 2C_i + 1 \right) & if (i,t,j,t') \in \overline{A} \text{ and } i \in S \end{cases} \quad (22)$$

In objective (22), $\vartheta^k_{i,t,j,t'} = \sum_{k' \in K/k} \sum_{(i,t,u,j,t',u') \in A_{k'}} x^{k'}_{i,t,u,j,t',u'} + \sum_{k' \in K/k} \sum_{(i,\tau,u,j,\tau',u') \in \psi(i,t,j,t')} x^{k'}_{i,\tau,u,j,\tau',u'}$ denotes the total occupation of arc (i,t,j,t') and its incompatible arcs, except for the current train k, and $\varphi^k_{i,t} = \sum_{k' \in K/k} \sum_{\tau \in T} \sum_{(i,\tau,0,i,t',0) \in A_{k'}} x^{k'}_{i,\tau,0,i,t',0} + \sum_{k' \in K/k} \sum_{(i,t,u,j,t',u') \in A_{k'}} x^{k'}_{i,t,u,j,t',u'}$ denotes the total station occupation of station i at time t, except for the current train k. Thus, the values of $\vartheta^k_{i,t,j,t'}$ and $\varphi^k_{i,t}$ are fixed when we reschedule train k.

The decomposed problem $\mathbf{M}^k_{\text{ADMM}}$ is a shortest-path search problem, and a DP algorithm can be used to solve it. $\widehat{c}^k_{itujt'u'}$ is the general cost of train k using an STS arc (i,t,u,j,t',u').

The iterative ADMM procedure used to solve the decomposed train rescheduling model is given in Algorithm 1.

Algorithm 1. ADMM algorithm to solve train rescheduling

Input:

The initial Lagrange multipliers $\mu^k_{i,t,j,t'}(0)$ and $\pi^t_i(0)$ and penalty parameters ρ_1 and ρ_2;

The initial iteration step $q = 0$;

The maximum iteration step Q.

For step $q \leq Q$:

For each train $k \in K$:

Find the time-dependent and speed-dependent shortest path for train k with the paths for other trains being fixed;

Update the general arc costs based on the new solution for train k and previous solutions for other trains.

End for

Update Lagrange multipliers $\mu^k_{i,t,j,t'}$ and π^t_i based on the following two equations:

$$\mu^k_{i,t,j,t'}(q+1) = \max\{0, \mu^k_{i,t,j,t'}(q) + \rho_1(q) \left(\sum_{k' \in K} \sum_{(i,t,u,j,t',u') \in A_{k'}} x^{k'}_{i,t,u,j,t',u'} + \sum_{(i,\tau,u,j,\tau',u') \in \psi(i,t,j,t')} x^k_{i,\tau,u,j,\tau',u'} - 1 \right)\}$$

$$\pi^t_i(q+1) = \max\{0, \pi^t_i(q) + \rho_2(q) \left(\sum_{k \in K} \sum_{\tau \in T} \sum_{(i,\tau,0,i,t',0) \in A_k} x^k_{i,\tau,0,i,t',0} + \sum_{k \in K} \sum_{(i,t,u,j,t',u') \in A_k} x^k_{i,t,u,j,t',u'} - C_i \right)\}$$

Update penalty parameters ρ_1 and ρ_2 using the following equation (Wang et al., 2012), where ϵ and λ are parameters and $conf^q$ is the total number of conflicts of headway and station capacity at iteration q. These parameters are explained later.

$$\rho(q+1) = \begin{cases} \rho(q) & \text{if} |conf^q| \leq \lambda |conf^{q-1}| \\ \epsilon \times \rho(q) & \text{if} |conf^q| > \lambda |conf^{q-1}| \end{cases}$$

Update iteration step: $q = q + 1$

End for

In Algorithm 1, we update the Lagrange multipliers and penalty parameters at each iteration. The functions used to update the penalty parameters are based on Wang et al. (2012), where parameter $\epsilon > 1$ and $0 < \lambda < 1$. $conf^q$ and $conf^{q-1}$ are the total numbers of conflicts of headway and station capacity constraints (constraints (3) and (4)) at iterations q and $q-1$, respectively. The procedure of

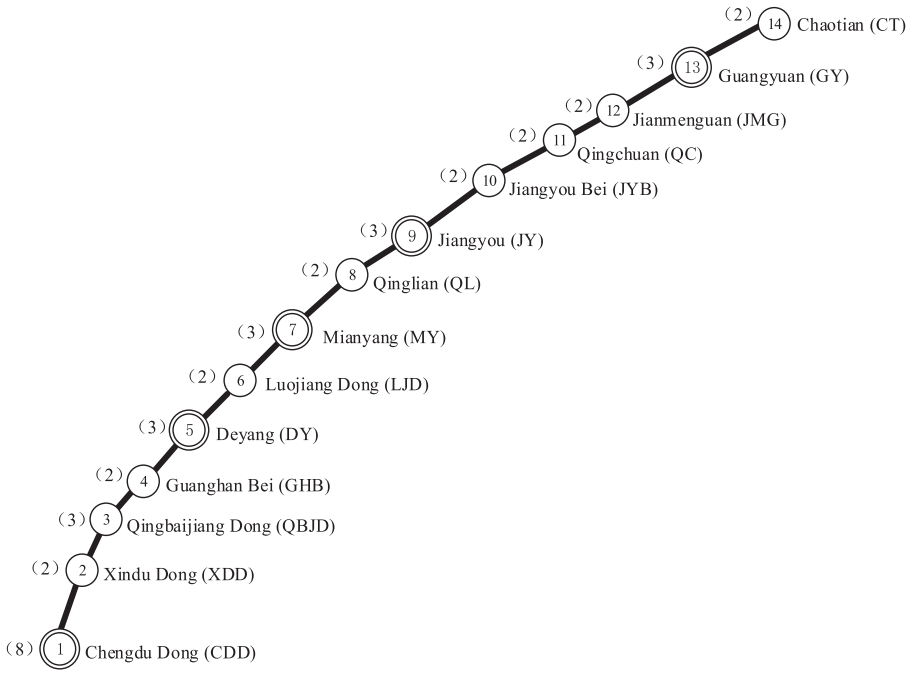

Fig. 5. Test part of the Xi'an–Chengdu high-speed railway line.

Table 3
Minimum and maximum running times in each segment.

No.	Segment	Distance (km)	Min run time (min)	Max run time (min)	Selected run times (min)
1	Chengdu Dong–Xindu Dong	21	6	11	6, 7, 8, 10, 11
2	Xindu Dong–Qingbaijiang Dong	11	3	6	3, 4, 5, 6
3	Qingbaijiang Dong–Guanghan Bei	14	4	7	4, 5, 6, 7
4	Guanghan Bei–Deyang	20	5	10	5, 6, 7, 9, 10
5	Deyang–Luojiang Dong	21	6	11	6, 7, 8, 10, 11
6	Luojiang Dong-Mianyang	26	7	13	7, 8, 9, 11, 13
7	Mianyang–Qinglian	25	6	13	6, 7, 8, 10, 12, 13
8	Qinglian–Jiangyou	14	4	7	4, 5, 6, 7
9	Jiangyou–Jiangyou Bei	37	9	19	9, 10, 11, 13, 15, 17, 19
10	Jiangyou Bei–Qingchuan	33	8	17	8, 9, 10, 12, 14, 16, 17
11	Qingchuan–Jianmenguan	18	5	9	5, 6, 7, 8, 9
12	Jianmenguan–Guangyuan	38	10	19	10, 11, 12, 14, 16, 18, 19
13	Guangyuan–Chaotian	38	10	19	10, 11, 12, 14, 16, 18, 19

tracking the total conflicts is given in Appendix D. Note that we use the same value for parameters ρ_1 and ρ_2 at each iteration. However, their values can also be set as different. To avoid over-increasing the values of parameters ρ_1 and ρ_2, we stop updating them when a feasible solution is obtained at a certain iteration. The time-dependent and speed-dependent shortest path for each train is found by using the DP algorithm described in Appendix A.

4. Case study

We first introduce the railway line and trains used in our test and the assumed disruption scenarios. We then test our models and algorithms in various disruption scenarios to investigate the trade-off between the train operation cost (energy cost) and train deviation cost. The train rescheduling model and algorithms are coded in Python 3.7. We run the experiments on an Intel Core i9-9900 K processor with a CPU running at 3.60 GHz (i.e., a 3.60-GHz 32.0-GB RAM desktop). The single-train trajectory optimization model is coded in MATLAB and run on a laptop with an Intel i7-7600U processor and 16 GB of RAM.

4.1. Test instance and parameter values

Our models and algorithms are tested on the Xi'an–Chengdu high-speed railway line in west China, which has many gradients and curves due to its location in a mountainous region. This line is served by two railway companies: China Railway Chengdu Group Co.,

Table 4
Possible speed levels for trains' arrival or departure at a station.

Speed level	1	2	3	4	5	6
Speed (km/h)	0	50	100	150	200	250
Speed (m/s)	0	14	28	42	56	70

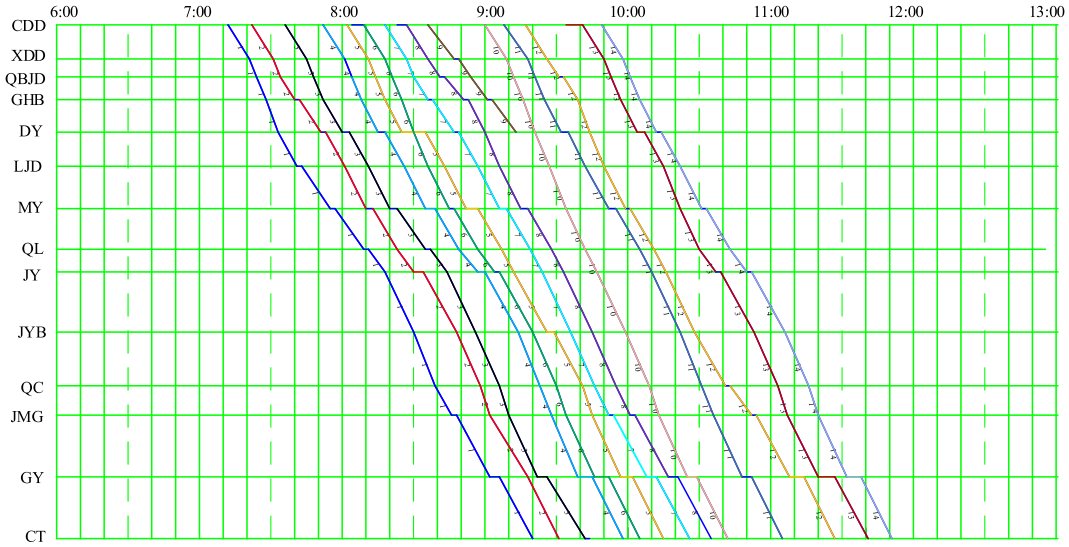

Fig. 6. Original timetable.

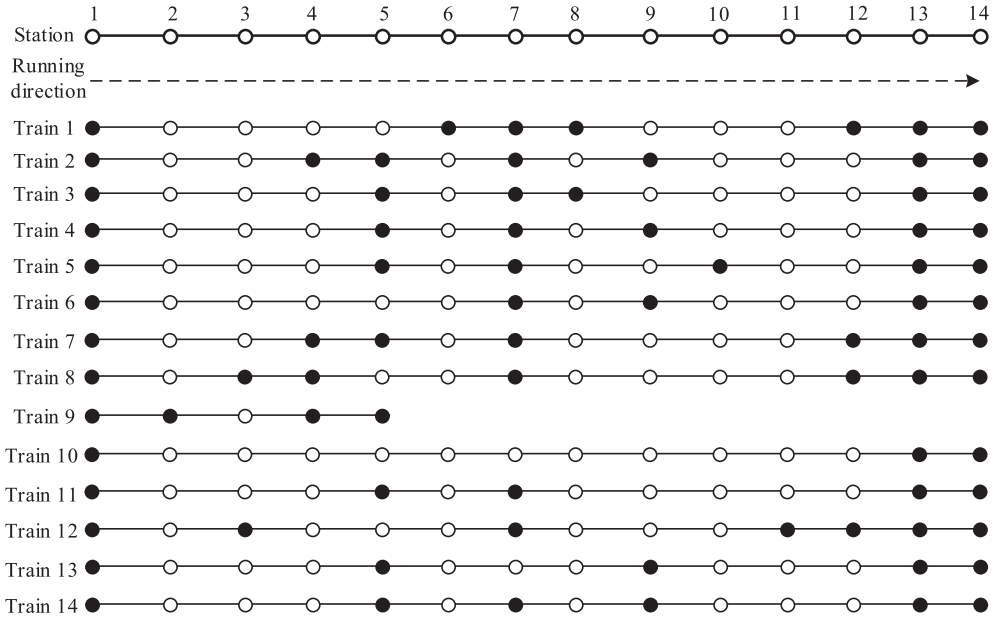

Fig. 7. Planned stopping patterns of trains.

Ltd. and China Railway Xi'an Group Co., Ltd. As we only have detailed information on this line for the portion served by the China Railway Chengdu Group Co., Ltd., this case study considers only the section from Chengdu Dong station to Chaotian station. This part of the high-speed railway line includes 14 stations and runs for 316 km. The section from Chengdu Dong station to Jiangyou station is also part of the Cheng–Mian–Le intercity high-speed railway line. Therefore, several terminal stations exist for the trains' original departure and final arrival in the intercity section. The railway line considered in this study is shown in Fig. 5, with the stations

Table 5
Detailed information on CRH380A.[1,2]

Characteristic	CRH380A (6M2T)
Train mass (t)	452
Rotating mass factor	1.06
Train length (m)	203
Maximum traction power (kW)	9600
Maximum traction force (kN)	213
Maximum braking rate (m/s^2)	0.98

Note: 6M2T means that six carriages have power and two carriages do not.
[1] https://wenku.baidu.com/view/6ce7a94855270722182ef747.html.
[2] https://wenku.baidu.com/view/5cffbb9ea31614791711cc7931b765-ce04087a1c.html.

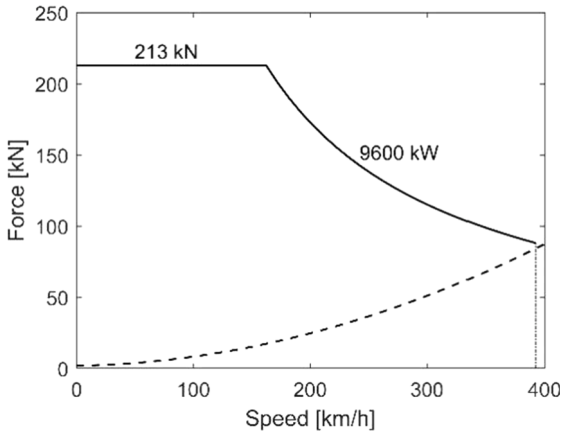

Fig. 8. Traction force (black line) and train resistance (dotted line) of a train using CRH380A as an EMU.

indicated by circles and the terminal stations indicated by double circles (the station number is inside the circle). The name of each station is abbreviated in brackets after its full name. The capacity of each station (C_i) is shown in brackets near each station.

Detailed information on the infrastructure of the considered line was obtained from the China Railway Chengdu Group Co., Ltd. and includes detailed gradients and curves. As the line is a double-track high-speed railway line, with each track occupied by trains running in one direction, we take the upstream line (Chengdu Dong–Chaotian) as an example in this case study. The problem for the other line can be handled in the same way.

Table 3 lists the distances between two consecutive stations on the line. The maximum running speed of this line is 250 km/h, and we assume that the minimum average speed is 120 km/h. The minimum and maximum running times of a train in each segment are shown in Table 3. The running time of a train in a segment varies between the minimum and maximum running times. In this case study, if the difference between the minimum and maximum running times is < 5 min, then we use 1 min as the interval to set the possible running times; otherwise, except for the first two possible running times, 2 min is used as the interval to select the possible running times, and the minimum and maximum running times are included (see the last column of Table 3). However, some running times may be infeasible; for example, if a train stops at the two end stations of a segment, it is impossible to run at the minimum running time due to the extra acceleration and deceleration times required for stopping. These impossible running times can be eliminated at the microscopic optimal train control stage, which can reduce the number of possible driving arcs. If a train is scheduled to stop at a given station, we assume that its dwell time is 2 min. The arrival and departure speeds of a train at a station are discretized into various speed levels; we assume six possible speed levels in this case study, with the speeds varying from 0 km/h to 250 km/h, in intervals of 50 km/h. The assumed speed levels are given in Table 4.

We consider trains that depart from their origins between 07:00 and 10:00. We do not consider trains departing throughout the day due to uncertainties in the disruptions and real-time requirements. The actual timetable used in 2020 states that 14 trains run on this line in the direction from Chengdu Dong to Chaotian during the 3-h period under consideration. Fig. 6 gives the original timetable for these 14 trains; each colored line denotes a train run, and the train number is shown next to the line to distinguish the various trains. The same labels are used in Figs. 13 and 14. Fig. 7 gives the running directions (from station 1 to station 14) and the scheduled stopping patterns of these trains. Note that because Chaotian (14) is the last station on our line, we assume that all trains stop there. In this figure, the stations are numbered from Chengdu Dong to Chaotian; a solid dot denotes that a train has a planned stop at this station and a hollow dot indicates that a train does not have a planned stop there. We assume that: (1) a disruption occurs on the segment between Mianyang and Qinglian (segment 7) at 08:00 and blocks the segment for 30 min, 60 min, or 90 min; and (2) a disruption occurs on the segment between Guanghan Bei and Deyang (segment 4) at 08:00 and blocks the segment for 30 min, 60 min, or 90 min. Therefore,

Table 6
Test results for various disruption scenarios with various weights of the two objectives.

Parameters(ω_1, ω_2)	Disruption scenario	Delay time (min)	Energy cost (kWh)	Extra stop	Best iteration	Feasible iteration	Computational time (s)
(1, 0)	(8,7,30)	157	48,331	15	2	2	(2,287, 228)
(1, 0.02)	(8,7,30)	240	31,808	0	4	3	(2,261, 452)
(1, 0.1)	(8,7,30)	1,003	24,600	0	7	5	(2,211, 773)
(1, 0.5)	(8,7,30)	2,310	19,198	0	10	9	(2,180, 1,090)
(1, 2.5)	(8,7,30)	2,802	18,611	0	2	2	(2,190, 219)
(1, 0)	(8,7,60)	1,248	47,752	17	16	13	(2,188, 1,750)
(1, 0.02)	(8,7,60)	1,520	32,027	4	17	16	(2,218, 1,885)
(1, 0.1)	(8,7,60)	2,010	25,014	2	15	13	(2,157, 1,617)
(1, 0.5)	(8,7,60)	3,129	19,083	0	17	10	(2,143, 1,821)
(1, 2.5)	(8,7,60)	3,573	18,611	0	12	11	(2,156, 1,293)
(1, 0)	(8,7,90)	2,977	49,201	22	16	15	(2,118, 1,694)
(1, 0.02)	(8,7,90)	3,296	33,047	5	18	16	(2,114, 1,902)
(1, 0.1)	(8,7,90)	4,229	24,149	6	18	13	(2,117, 1,905)
(1, 0.5)	(8,7,90)	4,712	19,563	3	15	13	(2,057, 1,542)
(1, 2.5)	(8,7,90)	5,239	18,617	2	11	10	(2,088, 1,148)
(0.5, 0)	(8,4,30)	340	48,612	17	9	8	(2,277, 1,024)
(1, 0.02)	(8,4,30)	614	31,913	4	10	7	(2,225, 1,112)
(1, 0.1)	(8,4,30)	1,416	24,744	3	11	11	(2,233, 1,228)
(1, 0.5)	(8,4,30)	2,345	19,593	2	12	6	(2,220, 1,332)
(1, 2.5)	(8,4,30)	3,068	18,611	1	12	11	(2,182, 1,309)
(1, 0)	(8,4,60)	1,867	49,207	21	17	12	(2,213, 1,881)
(1, 0.02)	(8,4,60)	2,243	33,721	8	20	18	(2,163, 2,163)
(1, 0.1)	(8,4,60)	2,838	25,142	7	11	10	(2,172, 1,194)
(1, 0.5)	(8,4,60)	3,949	19,674	5	18	14	(2,159, 1,943)
(1, 2.5)	(8,4,60)	4,716	18,652	1	16	14	(2,179, 1,743)
(1, 0)	(8,4,90)	4,786	50,337	32	28	13	(3,208, 2,994)
(1, 0.02)	(8,4,90)	5,043	33,117	11	16	12	(2,084, 1,667)
(1, 0.1)	(8,4,90)	5,925	24,486	15	17	13	(2,085, 1,772)
(1, 0.5)	(8,4,90)	6,441	19,961	10	16	14	(2,064, 1,651)
(1, 2.5)	(8,4,90)	7,179	18,852	6	18	17	(2,083, 1,874)

In Table 6, we extend the maximum number of iterative steps to 30 instead of 20 for the disruption scenario (8,4,90), with $\omega_1 : \omega_2 = 1 : 0$, because the feasible solution obtained within 20 iterations is inadequate, showing a train delay cost of 5,331 and energy cost of 50,161.

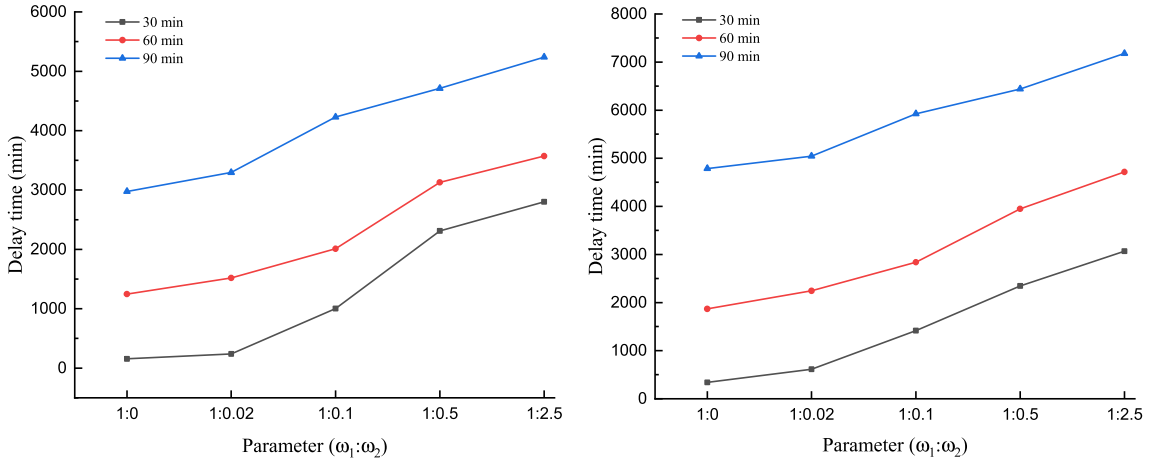

Fig. 9. Total train delay when the ratios of ω_1:ω_2 vary for disruptions with different durations.

trains cannot pass the disrupted segment during the period of disruption. To better investigate the trade-offs between train delay and energy consumption, we do not cancel trains.

In practice, 13 types of electric multiple units (EMUs) are used on this line, including CRH380A, CRH380B, CRH380D, CRH3A, and CRH2A. To simplify analysis, we assume that only CRH380A is used for our trains as it is generally preferred to use a single or only a few types of EMUs on a high-speed railway line to simplify train operations. Table 5 and Fig. 8 show detailed information on the type CRH380A EMUs with eight carriages. The trains considered in this case study are assumed to be eight-carriage trains.

We assume that both the minimum departure and arrival headways are 3 min. The initial Lagrange multipliers for μ and π are both

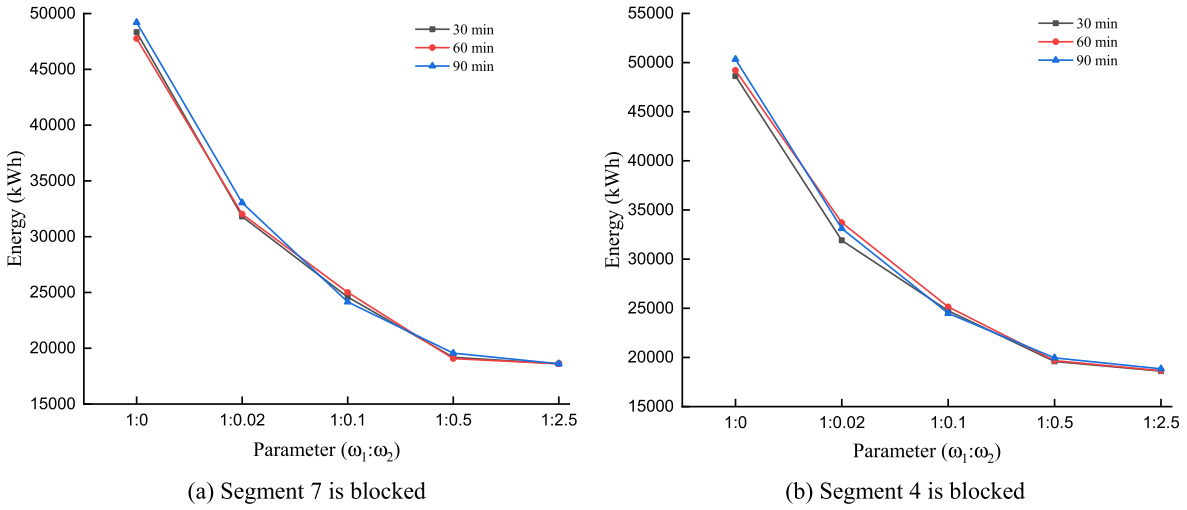

(a) Segment 7 is blocked (b) Segment 4 is blocked

Fig. 10. Total energy consumption when the ratios of ω_1:ω_2 vary for disruptions with different durations.

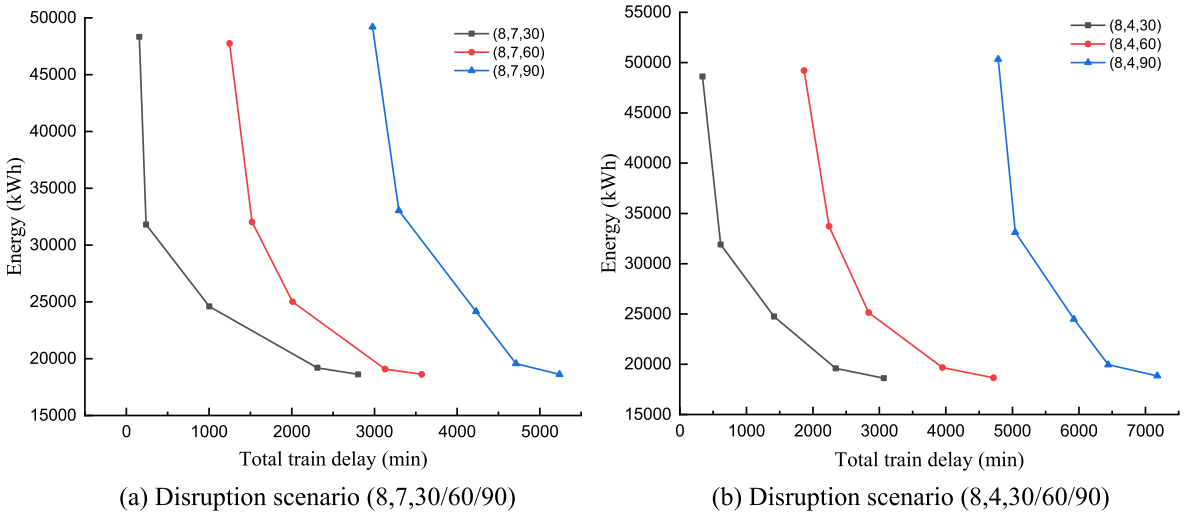

(a) Disruption scenario (8,7,30/60/90) (b) Disruption scenario (8,4,30/60/90)

Fig. 11. Trade-off between energy consumption and train arrival delay for various disruption scenarios.

0, and the initial quadratic penalty parameters ρ_1 and ρ_2 are both 10. The values of parameters ϵ and λ are assumed to be 1.5 and 0.5, respectively, to update the value of ρ in each iteration. As we investigate the trade-off between train operation cost (energy cost) and train delay cost, the ω_1:ω_2 parameter ratio varies in our tests. In practice, the train delay is a long-run cost leading to railway business loss if the delay is excessive. Delays may also cause railway passengers to lose confidence in high-speed railways and switch to other modes such as domestic flights. To quantify this cost and gauge the impact, railway companies may conduct a questionnaire survey. However, the energy consumption calculation is relatively straightforward, the cost of which can be obtained from the electricity bill. Based on these two costs, the railway company can select the best ratio for ω_1:ω_2. In our test, the value of parameter ω_1 is fixed to 1, whereas that of ω_2 varies (with values of 0, 0.02, 0.1, 0.5, and 2.5). Therefore, the ratios of ω_1:ω_2 are 1:0, 50:1, 10:1, 2:1, and 2:5. We limit the number of iterations to 20 to achieve a balance between computational time and solution quality.

4.2. Test results

In the test, we vary the values of ω_2, as mentioned above, to investigate the trade-off between delay recovery and energy saving. A ω_2 value of 0 means that we consider only the train delay and not the energy cost in train rescheduling. In this situation, our problem reduces to the traditional train rescheduling problem, with an objective of minimizing the train delay (Zhan et al., 2015). However, although the train delay can be minimized, the energy consumption may be large. Based on the test instances and parameters introduced in Section 4.1 and the values of ω_1 and ω_2 introduced above, we reschedule trains in each assumed disruption scenario in this section. By varying the values of ω_2 and the location and duration of disruptions, we obtain 30 test instances, i.e., 1 for each row in

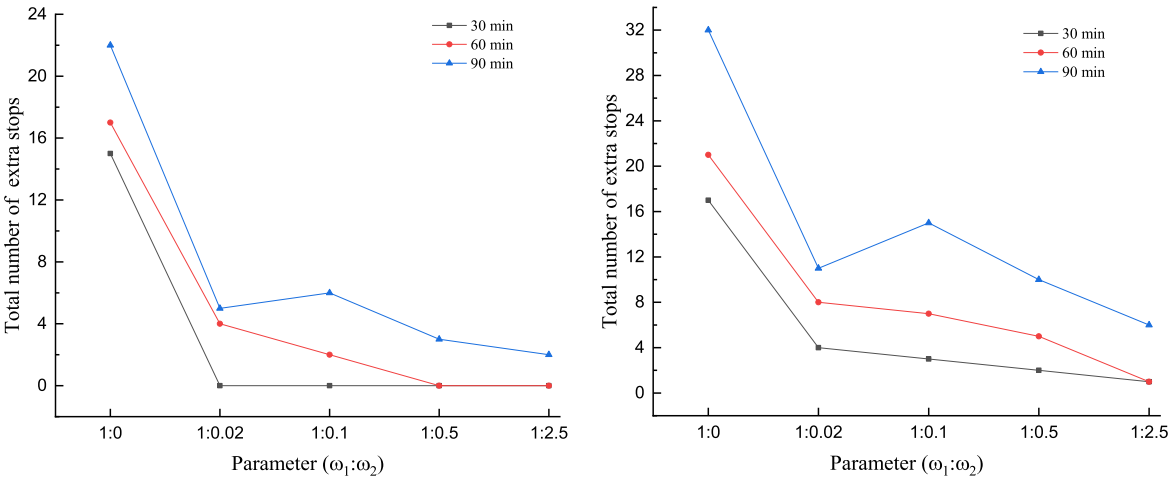

(a) Disruption scenario (8,7, 30/60/90) (b) Disruption scenario (8,4, 30/60/90)

Fig. 12. Total number of extra stops made by trains in each disruption scenario with different ratios of $\omega_1 : \omega_2$.

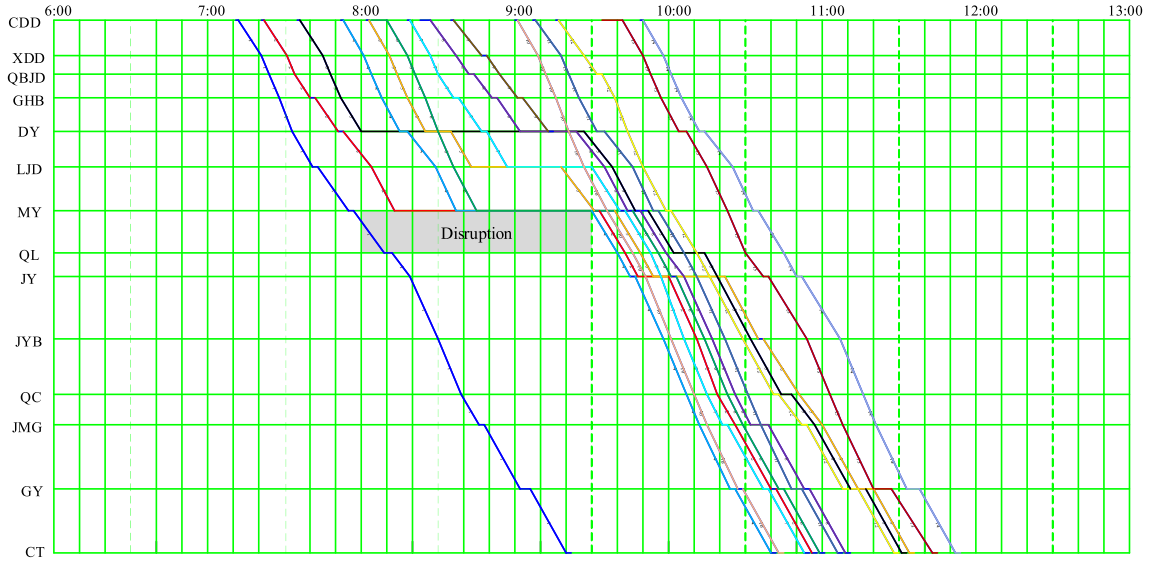

Fig. 13. Disposition timetable for disruption scenario (8,7,90) with $\omega_1 : \omega_2 = 1 : 0.02$.

Table 6.

The first column in Table 6 gives the values for parameters ω_1 and ω_2; the second column gives the disruption scenario, with the first number in the brackets denoting the disruption occurrence time (i.e., 08:00), the second number denoting the disrupted segment (i.e., segment 7 or segment 4), and the third number denoting the disruption duration (i.e., 30 min, 60 min, or 90 min); the third column is the total train arrival delay (min), which describes the total delay of each train that arrives at each station, as mentioned above; the fourth column shows the total energy consumption (kWh); the fifth column is the total number of extra stops made due to a disruption; the sixth and seventh columns are the iteration steps required to find the best solution and the first feasible solution within a 20-step limit, respectively; and the last column gives the total computational time, with the first number in the brackets denoting the total computational time taken for the 20 steps and the second number denoting the average computational time required to obtain the best found solution.

Table 6 shows that the total train delay increases with increasing ω_2, because increasing the value of ω_2 (decreasing the ratio of $\omega_1 : \omega_2$) implies that greater weightage is given to energy efficiency during train rescheduling (see Fig. 9 (a) and 9 (b)). In these two figures, 30 min, 60 min, and 90 min in the legend denote the duration of the disruptions, as in Figs. 10 and 12. However, the total energy consumption decreases with increasing ω_2 (see Fig. 10 (a) and 10 (b)). This means that if we account for the energy cost during

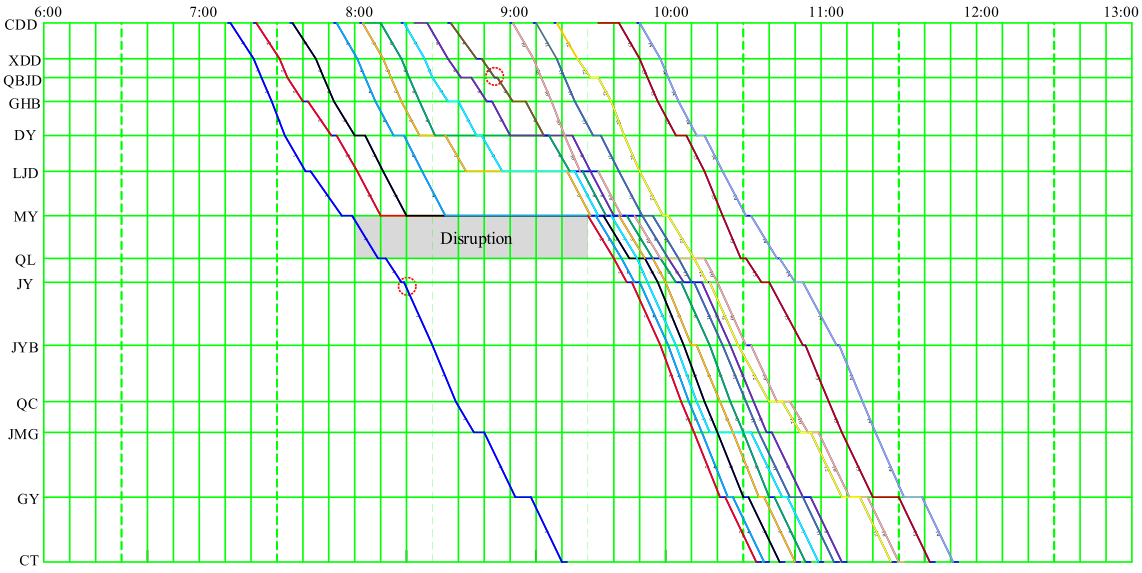

Fig. 14. Disposition timetable for disruption scenario (8,7,90) with $\omega_1 : \omega_2 = 1 : 0$.

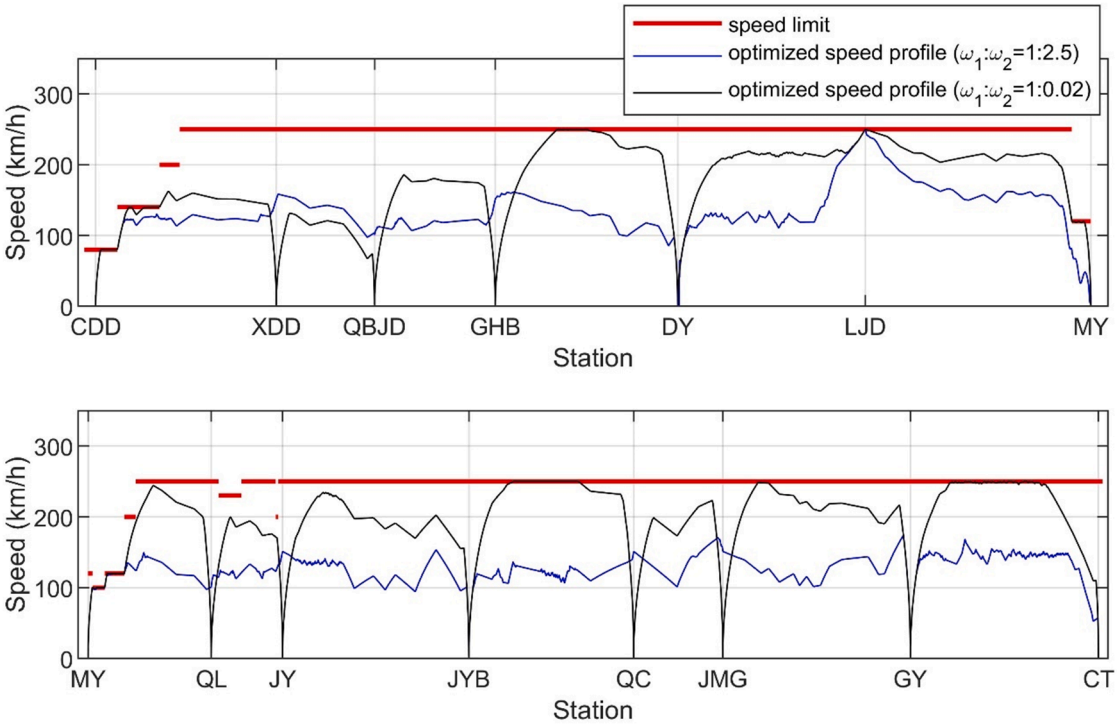

Fig. 15. Speed profile for Train 5 when $\omega_1 : \omega_2 = 1 : 2.5$ and $\omega_1 : \omega_2 = 1 : 0.02$.

train rescheduling, the total energy consumption is reduced significantly. Evidently, there is a trade-off between the train delay and energy efficiency.

Fig. 11 shows the trade-off for each disruption scenario. The energy consumption is reduced if we allow trains to have a larger delay, especially if we consider a small portion of the energy cost ($\omega_1 : \omega_2$ decreases from 1:0 to 1:0.02). If we allow trains to run slightly slower than their maximum speed, the energy consumption is reduced dramatically for all disruption scenarios. Specifically, by increasing the average total train delay by approximately 263.5 min (i.e., 18 min per train), the average energy consumption is reduced by $>$ 16,301 kWh (i.e., 33%). Therefore, from an energy efficiency perspective it is important to require trains to not run at their maximum speed during a disruption. However, the saving in energy consumption is reduced if we further increase the train delay by

Table 7
Comparison of the best feasible solution obtained using ADMM and the best lower bound obtained using LR.

Disruption scenario	Ratios of $\omega_1 : \omega_2$	Best feasible solution	Best LR lower bound	Gap (%)
(8,7,60)	1:0	1,248	866	30.6
	1:0.02	2,161	1,665	23.0
	1:0.1	4,511	4,164	7.7
	1:0.5	12,671	12,533	1.1
	1:2.5	50,074	49,956	0.2
(8,4,90)	1:0	4,786	3,487	27.1
	1:0.02	5,705	4,366	23.5
	1:0.1	8,374	7,038	16.0
	1:0.5	16,422	15,508	5.6
	1:2.5	54,309	53,163	2.1
Average				13.7

Table 8
The number of variables and constraints in the case study.

	Complexity	Number
Variable ($x^k_{i,t,u,j,t',u'}$)	$\|K\| \times \|L\| \times \|T\| \times \|V\| \times \|V\|$	27,941,760
Constraint (2)	$\|K\| \times (\|N\| - 2) \times \|T\| \times \|V\| + 2\|K\|$	1,209,628
Constraint (3)	$\|L\| \times \|T\| \times \|K\|$	776,160
Constraint (4)	$\|S\| \times \|T\|$	5,040
Constraint (5)	$\|K\| \times \|L_{drive}\| \times \|T\| \times \|V\|$	2,116,800

reducing the train speed (Fig. 11). Railway managers must select a suitable ratio of $\omega_1 : \omega_2$ to achieve a good balance between delay recovery and energy saving in the face of a disruption.

As mentioned previously, dispatchers can reduce the number of unnecessary stops made by trains and, thus, save energy by train rescheduling. We investigate the stopping patterns of the trains in each disruption scenario when different priorities are given to energy efficiency. The total numbers of extra stops made by the trains in each disruption scenario under various ratios of $\omega_1 : \omega_2$ are listed in the fifth column of Table 6 and shown in Fig. 12. Here, an extra stop refers to a stop that a train is not scheduled to make. The total number of extra stops generally decreases when the ratio of $\omega_1 : \omega_2$ decreases, implying that to save energy, train rescheduling must not result in extra train stops. If we focus only on minimizing the delay in train rescheduling ($\omega_1 : \omega_2 = 1 : 0$), then the trains are likely to stop at a higher number of stations, which is not desirable.

The disposition timetables for the disruption scenario (8,7,90), in which $\omega_1 : \omega_2 = 1 : 0.02$ and $\omega_1 : \omega_2 = 1 : 0$, are given as examples in Figs. 13 and 14, respectively. Note that train 1 departs from Mianyang Station before the disruption occurs, and we assume that it passes through the disrupted segment. It can be seen that the general features of the two disposition timetables are similar, in that the disrupted trains stop at some stations to wait until the disruption ends, and then run (separated by short intervals) after the disruption is resolved to try and meet their original schedules. However, the number of stops differs, as shown in Table 6. Here we choose two extra stops as an example (marked by red circles in Fig. 14) to illustrate that the trains are likely to make more extra stops when energy efficiency is not considered.

We also obtain the detailed speed profile for each rescheduled train during its journey in various disruption scenarios with various values of $\omega_1 : \omega_2$. This detailed speed profile can help guide the detailed train running process after a disruption. Without loss of generality, we use a specific train (Train 5) in a disruption scenario (8, 7, 90) with $\omega_1 : \omega_2 = 1 : 0.02$ and $\omega_1 : \omega_2 = 1 : 2.5$ as an example, to show the detailed train speed profiles (Fig. 15).

Fig. 15 shows that the real-time train speed does not exceed the speed limits, which are indicated by the red lines in the figure. Before the segment between Mianyang station and Qinglian station, the train runs at a relatively low speed (especially from Chengdu Dong to Guanghan Bei) due to the blockage of the segment between Mianyang and Qinglian. This situation is normal in railway practice, in which trains reduce their speed after a disruption. When we consider a low value of energy efficiency ($\omega_1 : \omega_2 = 1 : 0.02$; the black line in Fig. 15), the train runs at an average speed of > 200 km/h after the disrupted segment, which is reasonable for a high-speed railway with a designed speed of 250 km/h on a route with many curves and that passes over many mountains. However, when the main focus is on energy efficiency ($\omega_1 : \omega_2 = 1 : 2.5$; the blue line in Fig. 15), the train speed is rather low throughout its journey (approximately 130 km/h) as more emphasis is placed on energy savings than on delay minimization ($\omega_1 : \omega_2 = 1 : 2.5$). The low running speed reduces energy consumption but increases the train delay, as can be seen from Table 6. Current railway practices mandate that we reduce the train delay. Therefore, we recommend that accounting for energy consumption to a lower degree and placing more emphasis on the train delay will yield a good solution to the train rescheduling problem, i.e., the solution obtained when $\omega_1 : \omega_2 = 1 : 0.02$ is more appropriate for practical applications than that obtained when $\omega_1 : \omega_2 = 1 : 2.5$.

4.3. Test of the efficiency of the ADMM algorithm

To investigate the quality of the solutions obtained using the ADMM algorithm, we use LR to obtain the lower bound of each disruption scenario. The relaxation of the train rescheduling model ($\boldsymbol{M}$) by LR is akin to the relaxation of the model by ADMM ($\boldsymbol{M}_{\mathrm{ADMM}}$), but without the quadratic terms. The relaxed model and solution algorithm of LR used to obtain the lower bound are given in Appendix E.

We take the disruption scenarios (8,7,60) and (8,4,90) as examples to compare the best feasible solutions obtained by the ADMM algorithm with the best lower bound obtained by the LR algorithm, with different ratios of ω_1:ω_2. In the LR algorithm, we run 100 iterations for each disruption scenario, and choose the best lower bound. The comparison is given in Table 7, where the gap is the difference between the best feasible solution and the best LR lower bound, divided by the best feasible solution. We can see that for both the disruption scenarios (8,7,60) and (8,4,90), the gaps are relatively large when the ratio of $\omega_1 : \omega_2$ is high. This may be because the lower bound obtained by LR is not very good for either train scheduling or the rescheduling problem when delay is the objective, e.g., the optimality gap is $>$ 30% in Meng and Zhou (2014), and approximately 40% in Luan et al. (2017). In our case, the average optimality gap is 13.7%. For our train rescheduling problem, quickly obtaining a good feasible solution is more meaningful than obtaining an optimal solution over a long computational time. Thus, the quality of the obtained feasible solutions is acceptable for our real-time problem.

In addition, we compare our ADMM algorithm with CPLEX to evaluate the computational efficiency. However, our model is too large to solve using CPLEX even when only two trains are considered. We have run CPLEX for greater than 3 h, but no solution could be found. The computational difficulty of CPLEX is due to the presence of too many variables and constraints in this STS network-based model. A comparison between the LR-based algorithm and CPLEX for an STS network-based model on metro train scheduling, which is a problem similar to that in our study, in a small case study was made by Shang et al. (2018). Their test results also showed that CPLEX is inefficient in solving STS network-based models. The approximate numbers of variables and constraints of our train rescheduling model are shown in Table 8. In this table, $|K|$, $|L|$, $|T|$, and $|V|$ are the number of trains, the number of links, time horizon, and number of speed levels, respectively. $|N|$ is the number of nodes, $|S|$ is the number of stations, and $|L_{drive}|$ is the number of drive arcs.

5. Conclusions

We formulate the macroscopic train rescheduling and the microscopic train speed profile optimization in an integrated approach in the event of a major disruption. When rescheduling trains, we not only consider delays in train arrival, as many studies have done, but also energy efficiency. Therefore, we achieve a good balance between the trade-offs of train delay and energy consumption, which will help railway dispatchers obtain a more sustainable disposition timetable. In addition, we consider detailed line characteristics such as gradients, curves, and speed limit points when optimizing the energy-efficient single-train speed profile. This speed profile optimization is performed offline in advance, thereby reducing the computational complexity.

Our train rescheduling model is an ILP based on an STS hypernetwork, which is difficult to solve using a commercial solver. Therefore, we decompose it into single train rescheduling problems using the ADMM algorithm, and solve each subproblem using DP. We test the model and algorithm on the Xi'an–Chengdu high-speed railway line in west China. The results demonstrate that our approach can help obtain a more balanced disposition timetable that considers both train deviation and energy consumption. Specifically, if we allow trains to run at slightly lower speeds than their maximum speed, the energy consumption is reduced significantly. In our test case, by accounting for energy efficiency to a certain degree ($\omega_1 : \omega_2 = 1 : 0.02$), the average train delay is increased by 18 min per train, but the total energy consumption is reduced by 16,301 kWh (33%), compared with a situation in which only train deviation is considered. In addition, we find that the use of energy efficiency as the only objective function for train rescheduling is not practical as the train speeds are too low.

Although we solve the energy-efficient train rescheduling using a linear programming model, this is a complicated approach. We assume that if two trains have sufficient headway at the start and end stations of a segment, they do not conflict with each other in the segment. The appropriate headway can be further investigated from a microscopic level to improve the railway capacity and timetable robustness in a future study. In addition, we decompose our model into subproblems, and solve these using DP. However, the efficiency of DP could be improved with a heuristic beam search (Zhou and Zhong, 2007). The added consideration of regenerative braking in our energy-efficient train rescheduling problem would also be an interesting research direction. Finally, it may be interesting to account for passenger behavior in train scheduling (Zhan et al., 2020) and rescheduling (Zhan et al., 2021).

CRediT authorship contribution statement

Shuguang Zhan: Conceptualization, Methodology, Software, Writing – original draft. **Pengling Wang:** Conceptualization, Methodology, Writing – review & editing. **S.C. Wong:** Writing – review & editing, Supervision. **S.M. Lo:** Supervision.

Declaration of Competing Interest

The authors declare that they have no known competing financial interests or personal relationships that could have appeared to influence the work reported in this paper.

Acknowledgments

This work was supported by grants from the Research Grants Council of the Hong Kong Special Administrative Region, China [No. T32-101/15-R]; National Natural Science Foundation of China (NSFC) [No. 71701174, 72171198]; Key Scientific and Technological Project of Henan Province [No. 182102310799]; the Foundation of Henan Educational Committee [No. 18A580003], and Guangdong - Hong Kong - Macau Joint Laboratory Program of the 2020 Guangdong New Innovative Strategic Research Fund, Guangdong Science and Technology Department [No. 2020B1212030009]. The first author was supported by the Hong Kong Scholar Scheme 2017. The third author was supported by the Francis S Y Bong Endowed Professorship in Engineering. We also would like to thank China Railway Chengdu Group Co., Ltd. for providing the data.

Appendix A. Time-dependent and speed-dependent shortest-path algorithm for each train

Algorithm 2 Dynamic programming algorithm to solve time-dependent speed-dependent shortest-path problem

Input: An STS network $G = (E, A)$;
The original timetable for trains to be rescheduled and the space–time graph for train $k \in K$ in STS network;
The origin o_k and destination d_k for each rescheduled train k;
The earliest departure time e_k and latest arrival time l_k of train k;
The cost of an STS arc (i, t, u, j, t', u') used by a train k in STS network, $c^k_{iujt'u'}$ and $\overline{c}^k_{iujt'u'}$;
The disruption information (i.e., occurrence time, location, and duration).

Step 1: Initialization
For train $k = 1$ **to** $|K|$ // each train
For physical link $(i, j) = 1$ **to** $|L_k|$ // each link available for train k
For time $t = e_k$ **to** l_k // each time during the possible time frame of k
For speed $u = 0$ to $|V|$ // each possible speed
If $(i = o_k, t = e_k, u = 0)$ // the start node, time, and speed for train k
$\xi^k_{i,t,u} = 0$ //$\xi^k_{i,t,u}$ is the label for train k at node (i, t, u)
Else
$\xi^k_{i,t,u} = \infty$
End if
Set train node precedence $PN_{i,t,u} = -1$, time precedence $PT_{i,t,u} = -1$, speed precedence $PS_{i,t,u} = -1$
End for // speeds
End for // times
End for // links
End for // trains

Step 2: Forward-finding the best node on the shortest path
For train $k = 1$ **to** $|K|$
For node $i = 1$ **to** $|N|$
For time $t = e_k$ **to** l_k
If $i \in S$ and $j = i+1 \in S$ // (i, j) is a segment driving link
$t \geq dep_{k,i}$ // train departure time window (constraint (5))
Else
pass
For speed $u = 0$ to $|V|$
Derive feasible downstream node j for i, feasible downstream time t' for t, and feasible downstream speed u' for u based on the stopping pattern of train k;
Calculate the general cost $\hat{c}^k_{iujt'u'}$ of arc (i, t, u, j, t', u') according to Equation (22);
If $(\xi^k_{i,t,u} + \hat{c}^k_{iujt'u'} < \xi^k_{j,t',u'})$
$\xi^k_{j,t',u'} = \xi^k_{i,t,u} + \hat{c}^k_{iujt'u'}$ //update the cost of successor node (j, t', u')
$PN_{j,t',u'} = i$, $PT_{j,t',u'} = t$, $PS_{j,t',u'} = u$ // keep track of the precedent node, time, and speed
End if
End for // u
End for //t
End for // i
End for // k

Step 3: Backtrack the time-dependent and speed-dependent shortest path
Step 3.1: Find the last STS node of train k on its shortest path obtained by DP

(*continued on next page*)

(*continued*)

Algorithm 2 Dynamic programming algorithm to solve time-dependent speed-dependent shortest-path problem
Step 3.2: Backtrack from the last STS node to the first STS node of train k, according to the precedence relationship **Step 3.3:** Output the shortest-path backward and the corresponding cost

In Algorithm 2, we must ensure that a train dwells at a planned-stop station; that is, if a train planned to stop at a station, it must use a dwell arc at that station. If train k planned to stop at i and the arc preceding station node (i,t,u) is a driving arc, the successive arc $((i,t,u,j,t',u'))$ of node (i,t,u) must be a dwell arc; otherwise, it must be a driving arc (without a stop at i) or a stopping arc (with an extra stop at i, due to a disruption). In addition, when a train stops at a station, both its arrival and departure speeds at the station must be zero; otherwise, these speeds are positive. Finally, as mentioned before, we keep the schedules before the disruption unchanged for trains.

Appendix B. Optimal control model of a single train

Notation for the single-train optimal control model is given in Table 2.
The general single-train control model is formulated as follows (Wang et al., 2015; Wang and Goverde, 2016):

Table 2
Notation.

Notation	Description	Type
s	The location of a train on a link	Independent variable
$v(s)$	Train speed at location s	Dependent variable
$t(s)$	The time of a train arriving at location s	Dependent variable
$f(s), b(s)$	The traction and braking force at location s	Dependent variable
$R_{train}(v)$	The train resistance force at speed v	Dependent variable
$R_{line}(s)$	The line resistance force at location s	Dependent variable
F_{max}, B_{max},P_{max}	The maximum traction, braking force and traction power	Parameter
$V_{max}(s)$	The speed limitation at location s	Parameter
A_{min}, A_{max}	The minimum- and maximum-acceptable riding comfort	Parameter
s_0, s_f	The departure and arrival locations of a train on a link	Parameter
θ_1, θ_2	Either traction force or braking force is used, $\theta_1 \bullet \theta_2 = 0$	Binary parameters
ε	The rotating mass factor	Parameter
α, β, γ	The constant coefficients for train resistance	Parameter
g	The acceleration of gravity	Parameter

$$\frac{dv(s)}{ds} = \frac{\theta_1 f(s) - \theta_2 b(s) - R_{train}(v) - R_{line}(s)}{\varepsilon \cdot m \cdot v(s)} \tag{7}$$

$$\frac{dt(s)}{ds} = \frac{1}{v(s)} \tag{8}$$

Subject to

$$0 \le f(s) \le F_{max} \tag{9}$$

$$0 \le b(s) \le B_{max} \tag{10}$$

$$0 \le f(s) \cdot v(s) \le P_{max} \tag{11}$$

$$0 \le v(s) \le V_{max}(s) \tag{12}$$

$$A_{min} \le \frac{dv(s)}{dt(s)} \le A_{max} \tag{13}$$

$$v(s_0) = u, v(s_f) = u', t(s_0) = t, t(s_f) = t' \tag{14}$$

Equation (7) is derived from Newton's second law, and Equation (8) is the definition of speed. In Equation (7), if traction is used, $\theta_1 = 1$ and $\theta_2 = 0$; if braking force is used, $\theta_1 = 0$ and $\theta_2 = 1$. Train resistance $R_{train}(v)$ is mainly consist of wind resistance (Hansen and Pachl, 2014), which can be formulated as $R_{train}(v) = 0.001 \cdot \varepsilon \cdot m \cdot g \cdot (\alpha + \beta \cdot v + \gamma \cdot v^2)$. The line resistance consists of grade resistance

and curve resistance, which can be denoted as $R_{line}(s) = R_{grade} + R_{curve}$. Constraints (9) to (12) specify the domains of traction force, braking force, traction power, and train speed at position s, respectively. Constraint (13) indicates that the acceleration and deceleration rates must fall within the interval $[A_{min}, A_{max}]$ to ensure the passengers' riding comfort. Constraint (14) connects the microscopic train trajectory on a segment between two stations with the macroscopic train rescheduling in Section 2.3.1. The constraint denotes that the start and end times and speeds of a train in a segment (link) between two stations must be consistent, where s_0, t, u, s_f, t', u' is given by the STS arc (i,t,u,j,t',u'), $s_0 = i$ and $s_f = j$.

Appendix C. Proof of property 1:

$$\sum_{(i,t,j,t')} \mu^k_{i,t,j,t'} \sum_{(i,\tau,u,j,\tau',u')\in\psi(i,t,j,t')} x^k_{i,\tau,u,j,\tau',u'} = \sum_{(i,\tau,j,\tau')\in\psi(i,t,j,t')} \mu^k_{i,\tau,j,\tau'} \sum_{(i,t,u,j,t',u')} x^k_{i,t,u,j,t',u'}$$

To simplify the notations in the proof, a space–time speed arc (i,t,u,j,t',u') is denoted as a. Because the incompatibility of two arcs is independent of the speed, the speed dimension is omitted. Arc (i,t,j,t') in the property can be transferred to arc (i,t,u,j,t',u') by adding a speed dimension. A train k can use one arc at most (i,t,u,j,t',u') in segment (i,j). We assume that train k uses arc a_0, i.e., $x^k_{a_0} = 1$ and $x^k_a = 0$ when $a \neq a_0$. Thus, we have:

$$\sum_{(i,t,j,t')} \mu^k_{i,t,j,t'} \sum_{(i,\tau,u,j,\tau',u')\in\psi(i,t,j,t')} x^k_{i,\tau,u,j,\tau',u'} = \sum_a \mu^k_a \sum_{a'\in\psi(a)} x^k_{a'} = \sum_a \mu^k_a \sum_{a_0\in\psi(a)} x^k_{a_0} = \sum_{a\in\psi(a_0)} \mu^k_a x^k_{a_0} \sum_{(i,\tau,j,\tau')\in\psi(i,t,j,t')} \mu^k_{i,\tau,j,\tau'} \sum_{(i,t,u,j,t',u')} x^k_{i,t,u,j,t',u'} = \sum_{a\in\psi(a_0)} \mu^k_a x^k_{a_0}$$

Therefore, property 1 is held.

Appendix D. The procedure to count the total conflicts for updating parameter ρ

Initial conflict = 0
For each arc $(i,j,t,t') \in A_{drive}$: // space–time drive arc
  For each train $k \in K$:
    If train k uses space–time arc (i,j,t,t'):
      For arc $(i,j,\tau,\tau') \in A_{drive}$ and $(i,j,\tau,\tau') \in \psi(i,j,t,t')$:
        For $k' \in K$ and $k' \neq k$:
          If train k' uses space–time arc (i,j,τ,τ'):
            conflict = conflict + 1
For each time-expanded station node (i,t), $i \in S$: // each station at time t
  station_occupied[i][t] = 0 // initialize the station occupation to 0.
  For each arc $(i,j,t,t') \in A_{station}$: // $A_{station}$ includes station dwell arcs and stopping arcs, and driving arcs, which is explained in the model for constraint (4)
    For each train $k \in K$:
      If train k uses space–time arc (i,j,t,t'):
        station_occupied[i][t] += 1 // keep track the station occupation
        If arc (i,j,t,t') is a dwell arc: // a dwell arc lasts two minutes
          If train k uses space–time arc $(i,j,t-1,t')$:
            station_occupied[i][t] += 1 // a train dwells at time $t-1$, it will dwell at time t
  If station_occupied[i][t] > C_i: // the station capacity is exceeded.
    conflict = conflict + 1

Appendix E. Lagrangian relaxation model and algorithm

By relaxing the headway constraint (3) and the station capacity constraint (4), we obtain the following LR model (M_{LR}):
Min:

$$\omega_1 \times \left(\sum_{k\in K} \sum_{(i,t,u,j,t',u')\in A_k} c^k_{ituj t'u'} \times x^k_{i,t,u,j,t',u'} \right) + \omega_2 \times \left(\sum_{k\in K} \sum_{(i,t,u,j,t',u')\in A_k} \overline{c}^k_{ituj t'u'} \times x^k_{i,t,u,j,t',u'} \right)$$

$$+ \sum_{(i,t,j,t')} \sum_{k\in K} \mu^k_{i,t,j,t'} \left(\sum_{k'\in K} \sum_{(i,t,u,j,t',u')\in A_{k'}} x^{k'}_{i,t,u,j,t',u'} + \sum_{(i,\tau,u,j,\tau',u')\in\psi(i,t,j,t')} x^k_{i,\tau,u,j,\tau',u'} - 1 \right)$$

$$+ \sum_{i\in S} \sum_{t\in T} \pi^t_i \left(\sum_{k\in K} \sum_{\tau\in T} \sum_{(i,\tau,0,i,t',0)\in A_k} x^k_{i,\tau,0,i,t',0} + \sum_{k\in K} \sum_{(i,t,u,j,t',u')\in A_k} x^k_{i,t,u,j,t',u'} - C_i \right) \tag{20a}$$

subject to (2) and (6).

To obtain the best lower bound of the LR model, we need to solve its dual problem (M_{LRD}) as follows:

$Max_{\boldsymbol{\mu},\boldsymbol{\pi}} Min_{\boldsymbol{x}}$:

$$\begin{aligned}
&\omega_1 \times \left(\sum_{k\in K} \sum_{(i,t,u,j,t',u')\in A_k} c^k_{itujt'u'} \times x^k_{i,t,u,j,t',u'} \right) + \omega_2 \times \left(\sum_{k\in K} \sum_{(i,t,u,j,t',u')\in A_k} \bar{c}^k_{itujt'u'} \times x^k_{i,t,u,j,t',u'} \right) \\
&+ \sum_{(i,t,j,t')} \sum_{k\in K} \mu^k_{i,t,j,t'} \left(\sum_{k'\in K} \sum_{(i,t,u,j,t',u')\in A_{k'}} x^{k'}_{i,t,u,j,t',u'} + \sum_{(i,\tau,u,j,\tau',u')\in \psi(i,t,j,t')} x^k_{i,\tau,u,j,\tau',u'} - 1 \right) \\
&+ \sum_{i\in S} \sum_{t\in T} \pi^t_i \left(\sum_{k\in K} \sum_{\tau\in T} \sum_{(i,\tau,0,i,t',0)\in A_k} x^k_{i,\tau,0,i,t',0} + \sum_{k\in K} \sum_{(i,t,u,j,t',u')\in A_k} x^k_{i,t,u,j,t',u'} - C_i \right)
\end{aligned} \tag{20b}$$

subject to (2) and (6).

In the objective function (20b), we use $\boldsymbol{\mu}$ and $\boldsymbol{\pi}$ to denote the corresponding LR multipliers and $\boldsymbol{x}$ to denote the decision variable for simplifying the notations.

Like the ADMM approach, we can decompose the LR dual model (M_{LRD}) into subproblems, and each subproblem is for a single train. However, the main differences between LR approach and ADMM approach are that (1) no quadratic terms exist in the LR model, so that the objective function is easier to be decomposed; (2) each subproblem can be solved in parallel in LR instead of being solved sequentially in ADMM. The subproblem for a single train decomposed from LR is as follows:

Min:

$$\begin{aligned}
Z^{LR}_k = {} & \omega_1 \times \left(\sum_{(i,t,u,j,t',u')\in A_k} c^k_{itujt'u'} \times x^k_{i,t,u,j,t',u'} \right) + \omega_2 \times \left(\sum_{(i,t,u,j,t',u')\in A_k} \bar{c}^k_{itujt'u'} \times x^k_{i,t,u,j,t',u'} \right) \\
& + \sum_{(i,t,j,t')} \mu^k_{i,t,j,t'} \times \sum_{k'\in K} \sum_{(i,t,u,j,t',u')\in A_{k'}} x^{k'}_{i,t,u,j,t',u'} + \sum_{(i,t,j,t')} \mu^k_{i,t,j,t'} \sum_{(i,\tau,u,j,\tau',u')\in \psi(i,t,j,t')} x^k_{i,\tau,u,j,\tau',u'} \\
& + \sum_{i\in S} \sum_{t\in T} \pi^t_i \times \left(\sum_{\tau\in T} \sum_{(i,\tau,0,i,t',0)\in A_k} x^k_{i,\tau,0,i,t',0} + \sum_{(i,t,u,j,t',u')\in A_k} x^k_{i,t,u,j,t',u'} \right) = \check{c}^k_{itujt'u'} \times x^k_{i,t,u,j,t',u'}
\end{aligned} \tag{21b}$$

Algorithm 3 Lagrangian relaxation algorithm to solve train rescheduling

Input:

The nonnegative initial Lagrange multipliers $\mu^k_{i,t,j,t'}(0)$ and $\pi^t_i(0)$;

The initial lower bound $Lo(0) = -\infty$, and the best lower bound $Lo^*(0) = Lo(0)$;

The initial iteration step $q = 0$;

The maximum iteration step Q.

For step $q \le Q$:

For each train $k \in K$:

Find the time-dependent and speed-dependent shortest-path for train k by dynamic programming with the known values of multipliers.

End for

Calculate the lower bound $Lo(q)$ for the current iteration q;

Update the best found lower bound by the following equation:

$$Lo^*(q) = \begin{cases} Lo^*(q-1) \text{ if } Lo(q). > Lo^*(q-1) \\ Lo(q) \text{ if } Lo(q) \le Lo^*(q-1) \end{cases}$$

Update Lagrange multipliers $\mu^k_{i,t,j,t'}$ and π^t_i based on the following two equations:

$$\mu^k_{i,t,j,t'}(q+1) = \max\{0, \mu^k_{i,t,j,t'}(q) + (1/(q+1)) \times (\textstyle\sum_{k'\in K}\sum_{(i,t,u,j,t',u')\in A_{k'}} x^{k'}_{i,t,u,j,t',u'} + \sum_{(i,\tau,u,j,\tau',u')\in\psi(i,t,j,t')} x^k_{i,\tau,u,j,\tau',u'} - 1)\}$$

$$\pi^t_i(q+1) = \max\{0, \pi^t_i(q) + (1/(q+1)) \times (\textstyle\sum_{k\in K}\sum_{\tau\in T}\sum_{(i,\tau,0,i,t',0)\in A_k} x^k_{i,\tau,0,i,t',0} + \sum_{k\in K}\sum_{(i,t,u,j,t',u')\in A_k} x^k_{i,t,u,j,t',u'} - C_i)\}$$

Update iteration step: $q = q + 1$

End for

subject to (2) and (6),

where the general LR cost $\check{c}^{k}_{itujt'u'}$ is calculated by Equation (22a). In Equation (22a), arc $\overline{A}$ is a drive arc ($i \neq j$) as that in Equation (22).

$$\check{c}^{k}_{itujt'u'} = \begin{cases} \omega_1 \times c^{k}_{itujt'u'} + \omega_2 \times \overline{c}^{k}_{itujt'u'} & if (i,t,j,t') \notin \overline{A} \text{ and } i \notin S \\ \omega_1 \times c^{k}_{itujt'u'} + \omega_2 \times \overline{c}^{k}_{itujt'u'} + \sum_{k' \in K} \mu^{k'}_{i,t,j,t'} + \sum_{(i,\tau,j,\tau') \in \psi(i,t,j,t')} \mu^{k}_{i,\tau,j,\tau'} & if (i,t,j,t') \in \overline{A} \text{ and } i \notin S \\ \omega_1 \times c^{k}_{itujt'u'} + \omega_2 \times \overline{c}^{k}_{itujt'u'} + \pi^{t}_{i} & if (i,t,j,t') \notin \overline{A} \text{ and } i \in S \\ \omega_1 \times c^{k}_{itujt'u'} + \omega_2 \times \overline{c}^{k}_{itujt'u'} + \sum_{k' \in K} \mu^{k'}_{i,t,j,t'} + \sum_{(i,\tau,j,\tau') \in \psi(i,t,j,t')} \mu^{k}_{i,\tau,j,\tau'} + \pi^{t}_{i} & if (i,t,j,t') \in \overline{A} \text{ and } i \in S \end{cases} \tag{22a}$$

The iterative procedure of LR to solve the decomposed train-rescheduling model is given in Algorithm 3. The dynamic programming algorithm to find the time-dependent and speed-dependent shortest-path to a single train is the same as that shown in Appendix A.

References

Albrecht, A., Howlett, P., Pudney, P., Vu, X., Zhou, P., 2016a. The key principles of optimal train control Part 1: Formulation of the model, strategies of optimal type, evolutionary lines, location of optimal switching points. Transport. Res. B: Methodol. 94, 482–508.

Albrecht, A., Howlett, P., Pudney, P., Vu, X., Zhou, P., 2016b. The key principles of optimal train control—Part 2: Existence of an optimal strategy, the local energy minimization principle, uniqueness, computational techniques. Transport. Res. Part B: Methodol. 94, 509–538.

Boyd, S., Parikh, N., Chu, E., Peleato, B., Eckstein, J., 2011. Distributed optimization and statistical learning via the alternating direction method of multipliers. Foundat. Trends Mach. Learn. 3 (1), 1–122.

Cacchiani, V., Huisman, D., Kidd, M., Kroon, L., Toth, P., Veelenturf, L., Wagenaar, J., 2014. An overview of recovery models and algorithms for real-time railway rescheduling. Transport. Res. B: Methodol. 63, 15–37.

Canca, D., Zarzo, A., 2017. Design of energy-efficient timetables in two-way railway rapid transit lines. Transport. Res. Part B: Methodol. 102, 142–161.

Caprara, A., Fischetti, M., Toth, P., 2002. Modeling and solving the train timetabling problem. Oper. Res. 50 (5), 851–861.

Corman, F., Meng, L., 2015. A review of online dynamic models and algorithms for railway traffic management. IEEE Trans. Intell. Transp. Syst. 16 (3), 1274–1284.

Cucala, A.P., Fernández, A., Sicre, C., Domínguez, M., 2012. Fuzzy optimal schedule of high speed train operation to minimize energy consumption with uncertain delays and driver's behavioral response. Eng. Appl. Artif. Intell. 25 (8), 1548–1557.

Fang, W., Yang, S., Yao, X., 2015. A survey on problem models and solution approaches to rescheduling in railway networks. IEEE Trans. Intell. Transp. Syst. 16 (6), 2997–3016.

Ghaemi, N., Cats, O., Goverde, R.M.P., 2018. Macroscopic multiple-station short-turning model in case of complete railway blockages. Transport. Res. Part C: Emerg. Technol. 89, 113–132.

Goverde, R.M.P., Bešinović, N., Binder, A., Cacchiani, V., Quaglietta, E., Roberti, R., Toth, P., 2016. A three-level framework for performance-based railway timetabling. Transport. Res. Part C: Emerg. Technol. 67, 62–83.

Hansen, I.A., Pachl, J., 2014. Railway timetabling & operations. Eurailpress, Hamburg.

Howlett, P., Pudney, P., 2012. Energy-efficient train control. Springer.

Kuppusamy, P., Venkatraman, S., Rishikeshan, C.A., Padmanabha Reddy, Y.C.A., 2020. Deep learning based energy efficient optimal timetable rescheduling model for intelligent metro transportation systems. Phys. Commun. 42, 101131. https://doi.org/10.1016/j.phycom.2020.101131.

Li, W., Peng, Q., Wen, C., Wang, P., Lessan, J., Xu, X., 2020. Joint optimization of delay-recovery and energy-saving in a metro system: a case study from China. Energy 202, 117699. https://doi.org/10.1016/j.energy.2020.117699.

Li, X., Lo, H.K., 2014. An energy-efficient scheduling and speed control approach for metro rail operations. Transport. Res. B: Methodol. 64, 73–89.

Liu, P., Yang, L., Gao, Z., Huang, Y., Li, S., Gao, Y., 2018. Energy-efficient train timetable optimization in the subway system with energy storage devices. IEEE Trans. Intell. Transp. Syst. 19 (12), 3947–3963.

Louwerse, I., Huisman, D., 2014. Adjusting a railway timetable in case of partial or complete blockades. Eur. J. Oper. Res. 235 (3), 583–593.

Luan, X., Miao, J., Meng, L., Corman, F., Lodewijks, G., 2017. Integrated optimization on train scheduling and preventive maintenance time slots planning. Transport. Res. C: Emerg. Technol. 80, 329–359.

Meng, L., Zhou, X., 2014. Simultaneous train rerouting and rescheduling on an n-track network: a model reformulation with network-based cumulative flow variables. Transport. Res. B: Methodol. 67, 208–234.

Montrone, T., Pellegrini, P., Nobili, P., 2018. Real-time energy consumption minimization in railway networks. Transport. Res. D: Transp. Environ. 65, 524–539.

Scheepmaker, G.M., Goverde, R.M.P., 2015. The interplay between energy-efficient train control and scheduled running time supplements. J. Rail Transp. Plann. Manage. 5 (4), 225–239.

Scheepmaker, G.M., Goverde, R.M.P., Kroon, L.G., 2017. Review of energy-efficient train control and timetabling. Eur. J. Oper. Res. 257 (2), 355–376.

Scheepmaker, G.M., Pudney, P.J., Albrecht, A.R., Goverde, R.M.P., Howlett, P.G., 2020. Optimal running time supplement distribution in train schedules for energy-efficient train control. J. Rail Transp. Plann. Manage. 14, 100180. https://doi.org/10.1016/j.jrtpm.2020.100180.

Shang, P., Li, R., Liu, Z., Yang, L., Wang, Y., 2018. Equity-oriented skip-stopping schedule optimization in an oversaturated urban rail transit network. Transport. Res. C: Emerg. Technol. 89, 321–343.

Sicre, C., Cucala, P., Fernández, A., Jiménez, J.A., Ribera, I., Serrano, A., 2010. A method to optimise train energy consumption combining manual energy efficient driving and scheduling. WIT Trans. Built Environ 114, 549–560.

Veelenturf, L.P., Kidd, M.P., Cacchiani, V., Kroon, L.G., Toth, P., 2016. A railway timetable rescheduling approach for handling large-scale disruptions. Transport. Sci. 50 (3), 841–862.

Wang, P., Goverde, R.M.P., 2016. Multiple-phase train trajectory optimization with signalling and operational constraints. Transport. Res. Part C: Emerg. Technol. 69, 255–275.

Wang, P., Goverde, R.M.P., 2017. Multi-train trajectory optimization for energy efficiency and delay recovery on single-track railway lines. Transport. Res. B: Methodol 105, 340–361.

Wang, P., Goverde, R.M.P., 2019. Multi-train trajectory optimization for energy-efficient timetabling. Eur. J. Oper. Res. 272 (2), 621–635.

Wang, P., Goverde, R.M.P., Ma, L., 2015. A multiple-phase train trajectory optimization method under real-time rail traffic management. In: In 2015 IEEE 18th International Conference on Intelligent Transportation Systems, pp. 771–776.

Wang, W., Xu, M., Fadel, G., Blouin, V., 2012. A consensus optimization via alternating direction method of multipliers for network target coordination. In 12th AIAA Aviation Technology, Integration, and Operations (ATIO) Conference and 14th AIAA/ISSMO Multidisciplinary Analysis and Optimization Conference, Indianapolis, IN, Paper No. AIAA 2012-5552.
Xu, P., Corman, F., Peng, Q., 2016. Analyzing railway disruptions and their impact on delayed traffic in Chinese high-speed railway. IFAC-Papers On Line 49 (3), 84–89.
Xu, Y., Jia, B., Li, X., Li, M., Ghiasi, A., 2020. An integrated micro-macro approach for high-speed railway energy-efficient timetabling problem. Transport. Res. Part C: Emerg. Technol. 112, 88–115.
Yang, G., Zhang, F., Gong, C., Zhang, S., 2019a. Application of a deep deterministic policy gradient algorithm for energy-aimed timetable rescheduling problem. Energies 12 (18), 3461.
Yang, X., Chen, A., Wu, J., Gao, Z., Tang, T., 2019b. An energy-efficient rescheduling approach under delay perturbations for metro systems. Transportmetrica B: Transp. Dyn. 7 (1), 386–400.
Ye, H., Liu, R., 2017. Nonlinear programming methods based on closed-form expressions for optimal train control. Transport. Res. C: Emerg. Technol. 82, 102–123.
Zhan, S., Kroon, L.G., Veelenturf, L.P., Wagenaar, J., 2015. Real-time high-speed train rescheduling in case of a complete blockade. Transport. Res. Part B: Methodol. 78, 182–201.
Zhan, S., Kroon, L.G., Zhao, J., Peng, Q., 2016. A rolling horizon approach to the high speed train rescheduling problem in case of a partial segment blockage. Transport. Res. Part E: Logist. Transport. Rev. 95, 32–61.
Zhan, S., Wong, S.C., Lo, S.M., 2020. Social equity-based timetabling and ticket pricing for high-speed railways. Transport. Res. Part A: Pol. Pract. 137, 165–186.
Zhan, S., Wong, S.C., Shang, P., Peng, Q., Xie, J., Lo, S.M., 2021. Integrated railway timetable rescheduling and dynamic passenger routing during a complete blockage. Transport. Res. B: Methodol. 143, 86–123.
Zhou, L., Tong, L.C., Chen, J., Tang, J., Zhou, X., 2017. Joint optimization of high-speed train timetables and speed profiles: a unified modelling approach using space-time-speed grid network. Transport. Res. B: Methodol. 97, 157–181.
Zhou, X., Zhong, M., 2007. Single-track train timetabling with guaranteed optimality: Branch-and-bound algorithms with enhanced lower bounds. Transport. Res. B: Methodol. 41, 320–341.
Zhu, Y., Goverde, R.M.P., 2019. Railway timetable rescheduling with flexible stopping and flexible short-turning during disruptions. Transport. Res. B: Methodol. 123, 149–181.